© 2016. Published by The Company of Biologists Ltd | Journal of Cell Science (2016) 129, 3412-3425 doi:10.1242/jcs.195867

RESEARCH ARTICLE

Persistent nuclear actin filaments inhibit transcription by RNA polymerase II

Leonid A. Serebryannyy[1], Megan Parilla[1], Paolo Annibale[2], Christina M. Cruz[1], Kyle Laster[3], Enrico Gratton[2], Dmitri Kudryashov[4], Steven T. Kosak[3], Cara J. Gottardi[5] and Primal de Lanerolle[1,*]

ABSTRACT

Actin is abundant in the nucleus and it is clear that nuclear actin has important functions. However, mystery surrounds the absence of classical actin filaments in the nucleus. To address this question, we investigated how polymerizing nuclear actin into persistent nuclear actin filaments affected transcription by RNA polymerase II. Nuclear filaments impaired nuclear actin dynamics by polymerizing and sequestering nuclear actin. Polymerizing actin into stable nuclear filaments disrupted the interaction of actin with RNA polymerase II and correlated with impaired RNA polymerase II localization, dynamics, gene recruitment, and reduced global transcription and cell proliferation. Polymerizing and crosslinking nuclear actin *in vitro* similarly disrupted the actin–RNA-polymerase-II interaction and inhibited transcription. These data rationalize the general absence of stable actin filaments in mammalian somatic nuclei. They also suggest a dynamic pool of nuclear actin is required for the proper localization and activity of RNA polymerase II.

KEY WORDS: Actin, Nuclear actin filaments, Nucleus, RNA polymerase II, Transcription

INTRODUCTION

Actin is one of the most evolutionarily conserved and abundant cellular proteins (Pollard and Cooper, 2009). Cytoplasmic actin has been studied for decades and is known to provide mechanical support and to power a host of cellular responses. Actin is also found in the nucleus and is integral to many nuclear processes (reviewed in de Lanerolle, 2012; de Lanerolle and Serebryannyy, 2011; Grosse and Vartiainen, 2013). Actively imported and exported, nuclear actin is a cofactor for several chromatin remodelers, transcription complexes, RNA-binding proteins and all three RNA polymerases. In the cytoplasm, the ability of actin to polymerize and depolymerize, which is crucial for its physiological functions (Pollard and Cooper, 2009), is sensitively regulated. Many of the same regulators of actin polymerization shuttle into the nucleus, suggesting that actin dynamics are also key to its nuclear functions (de Lanerolle and Serebryannyy, 2011; Gettemans et al., 2005; Grosse and Vartiainen, 2013).

[1]Department of Physiology and Biophysics, University of Illinois at Chicago, Chicago, IL 60612, USA. [2]Laboratory of Fluorescence Dynamics, University of California Irvine, Irvine, CA 92697, USA. [3]Department of Cell and Molecular Biology, Northwestern University, Chicago, IL 60611, USA. [4]Department of Chemistry and Biochemistry, Ohio State University, Columbus, OH 43210, USA. [5]Department of Medicine, Northwestern University, Chicago, IL 60611, USA.

*Author for correspondence (primal@uic.edu)

P.A., 0000-0003-3208-5347; E.G., 0000-0002-6450-7391; C.J.G., 0000-0003-0912-7617; P.deL., 0000-0001-8077-4273

Received 25 July 2016; Accepted 27 July 2016

New actin probes (Baarlink et al., 2013; Belin et al., 2013) and fluorescence recovery after photobleaching (FRAP) studies (McDonald et al., 2006) have indicated that actin exists in monomers and short polymers throughout the nucleus. Nuclear actin polymerization has been implicated in cellular differentiation (Sen et al., 2015), DNA damage clearance (Belin et al., 2015) and adenoviral replication (Fuchsova et al., 2015). Transient actin filaments, detected in nuclei upon serum stimulation or cell spreading, are reported to regulate the MAL (also known as MRTF) transcription factor pathway (Baarlink et al., 2013; Plessner et al., 2015). However, their effects on general transcription and chromatin remodeling are poorly understood. Notably, nuclear actin filaments are generally not observed and the use of exogenous probes to visualize nuclear actin polymerization might artificially promote actin assembly (Belin et al., 2013; Courtemanche et al., 2016; Du et al., 2015; Spracklen et al., 2014).

The polymerization of nuclear actin into dense, stable and phalloidin-stainable nuclear actin filaments occurs in some pathological conditions, such as skeletal myopathies (Domazetovska et al., 2007b), baculovirus infection (Goley et al., 2006) and idiopathic inflammatory myopathy (Stenzel et al., 2015). Nuclear actin filaments have also been noted following treatment with actin-depolymerizing drugs (Belin et al., 2013; Sen et al., 2015; Yahara et al., 1982) and upon dysregulation of actin-binding proteins such as exportin-6 (Dopie et al., 2015, 2012) and MICAL-2 (Lundquist et al., 2014). Furthermore, acute cellular stress, such as heat shock, as well as huntingtin mutations, lead to the formation of micron long actin and cofilin nuclear rods (Munsie et al., 2011; Nishida et al., 1987). Oocytes present a special situation where nuclear actin filaments confer structural stability to the large oocyte nucleus (Feric and Brangwynne, 2013). Oocytes also require nuclear actin polymerization for gene reprogramming (Miyamoto et al., 2011). However, stable, phalloidin-staining actin filaments are absent in normal mammalian somatic nuclei and their impact upon the nucleus in pathological conditions is unclear.

The role of nuclear actin in regulating general transcription has been studied extensively. Actin associates and co-purifies with RNA polymerases I, II and III and stimulates the activity of all three RNA polymerases *in vitro* (Hofmann et al., 2004; Hu et al., 2004; Philimonenko et al., 2004). Furthermore, nuclear actin is recruited to promoters with all three RNA polymerases in an activity-dependent manner (Hofmann et al., 2004; Hu et al., 2004; Philimonenko et al., 2004). In addition, *in vitro* translation studies have shown that β-actin directly interacts with at least three RNA polymerase III subunits: RPC3, RPABC2 and RPABC3 (Hu et al., 2004). Two of these subunits are components of all three RNA polymerases and might constitute conserved sites of nuclear actin binding. RNA polymerase I has been shown to require both actin and nuclear myosin I motor activity (Ye et al., 2008). RNA polymerase II (RNAPII) also requires actin and nuclear myosin I,

Journal of Cell Science

Journal of Cell Science (2016) 129, 3412-3425 doi:10.1242/jcs.195867

and actin is part of the pre-initiation complex (Hofmann et al., 2004, 2006). However, the form of actin necessary for RNAPII activity remains unclear (de Lanerolle and Serebryannyy, 2011; Grosse and Vartiainen, 2013).

We report here that formation of stable nuclear actin filaments correlated with altered RNAPII dynamics and localization. Sequestering endogenous monomeric nuclear actin by forming nuclear actin filaments reduced the association of RNAPII with nuclear actin and inhibited the recruitment of RNAPII to activated promoters, ultimately inhibiting transcription and proliferation. Similarly, polymerizing or crosslinking nuclear actin was able to impair the actin–RNAPII interaction and inhibit transcription *in vitro*. Taken together, our data suggest that maintaining nuclear actin in a non-filamentous state is critical for the functional integrity of the nucleus and shed mechanistic insight into the absence of classical actin filaments in the normal somatic nucleus.

RESULTS

Nuclear actin filaments sequester nucleoplasmic actin

The absence of classical actin filaments, despite the identification of many actin regulatory proteins in the nucleus, suggests that nuclear actin polymerization is tightly regulated. Therefore, we asked how stabilizing actin filaments in the nucleus would affect nuclear functions. We stabilized nuclear actin filaments by mutating actin (V163M-α-actin) or by bundling nuclear actin (with a fragment of supervillin, amino acids 1–1010) (Fig. 1A–C). V163M, one of many naturally occurring point mutations in α-skeletal muscle actin that cause the human disease intranuclear rod myopathy, is hallmarked by the formation of nuclear actin filaments (Domazetovska et al., 2007b) (Fig. 1B). Supervillin, a membrane-associated protein with multiple endogenous nuclear localization sequences (NLS), is an actin-bundling protein that regulates p53 levels and nuclear androgen receptor activity in prostate cancer (Fang and Luna, 2013; Ting et al., 2002; Wulfkuhle et al., 1999). Expressing a fragment of supervillin (Fig. 1C) resulted in the polymerization of endogenous actin into stable nuclear actin filaments that can be stained with phalloidin. Because of their association with several human diseases, these proteins represent pathologically relevant models for studying actin polymerization in the nucleus.

To quantify the effects of nuclear actin filaments on the dynamics of the nucleoplasmic pool of actin, we performed FRAP studies on COS7 cells using the EYFP–NLS-β-actin construct as a reporter as previously described (McDonald et al., 2006). Because targeting EYFP–β-actin to the nucleus can result in actin filaments in some cells (Fig. 1D), we photobleached ∼1 μm^2 areas devoid of any filaments in nuclei with and without nuclear actin filaments (Fig. 1E). Quantification of the recovery dynamics showed that nuclei with actin filaments had significantly increased half-lives of recovery and lower mobile fractions (Fig. 1F; Table S1A). Similar results were obtained from FRAP analyses on nuclei of cells transfected with wild-type EYFP–β-actin alone or in combination with the mCherry–supervillin fragment (Fig. S1A,B). Wild-type EYFP–β-actin did not form nuclear actin filaments alone but was readily incorporated into nuclear actin filaments when co-transfected with the supervillin fragment. This allowed us to

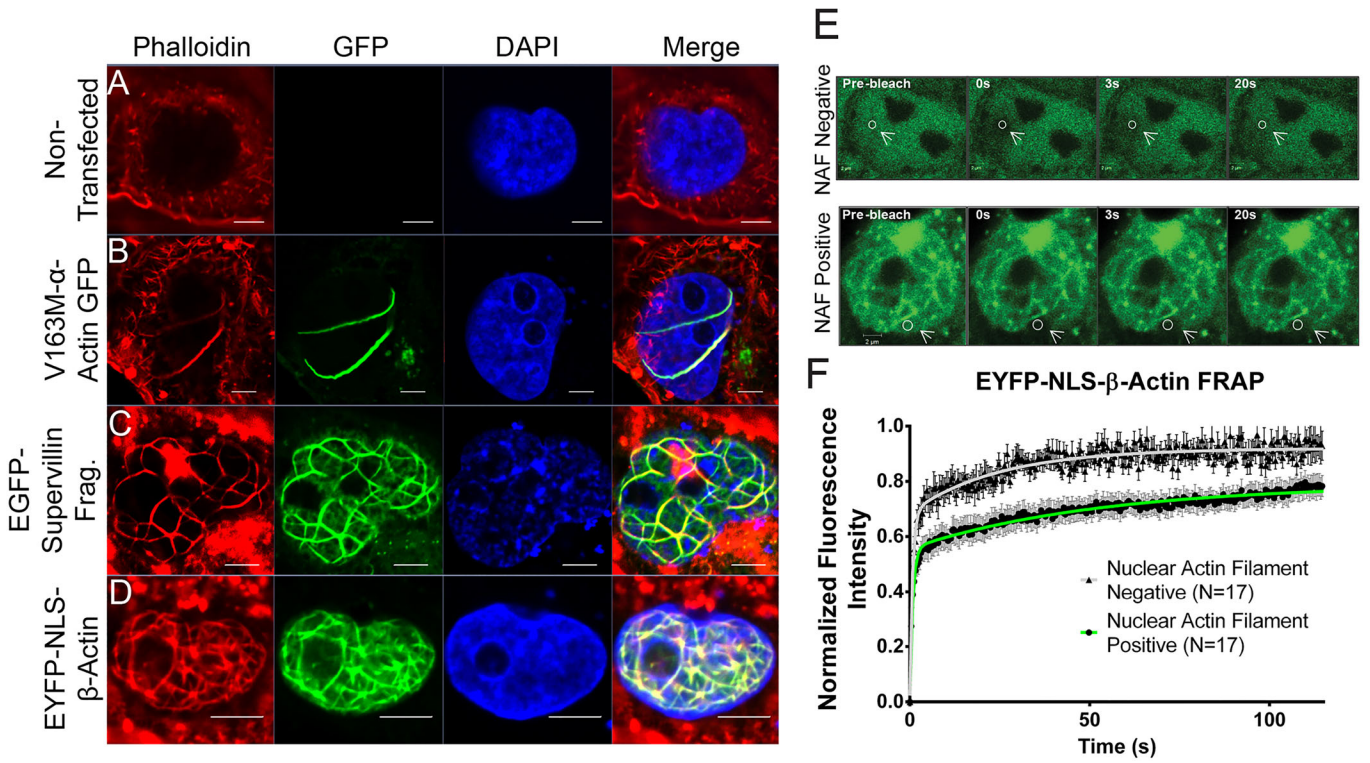

Fig. 1. The effects of nuclear actin filaments on nucleoplasmic actin. (A) Non-transfected cells or COS7 cells transfected with (B) V163M-α-actin–GFP, (C) the EGFP–supervillin fragment or (D) EYFP–NLS-β-actin (all shown in green) form large phalloidin-stained (red) actin filaments throughout the nucleus (blue). Scale bars: 5 μm. (E) FRAP experiment performed on COS7 cells transfected with EYFP–NLS-β-actin for 48 h. Areas of diffuse nuclear EYFP–β-actin were bleached in transfected cells (white circle and arrow) that had [nuclear actin filament (NAF) positive] and did not have (NAF negative) nuclear actin filaments. (F) FRAP analysis of nuclear pools of EYFP–β-actin fitted to a biphasic exponential recovery curve. Results are mean±s.e.m. Nuclear-actin-filament-positive nuclei (green) exhibit substantially longer recovery kinetics than those without filaments (nuclear actin filament negative; gray). FRAP kinetics are listed in Table S1A.

Journal of Cell Science

Journal of Cell Science (2016) 129, 3412-3425 doi:10.1242/jcs.195867

analyze actin dynamics in nuclei both without nuclear actin filaments and with nuclear actin filaments induced by nuclear actin bundling. Analysis of the data in Fig. 1F and Fig. S1A showed that the curves can be superimposed (R^2=0.88 and 0.89, when the curves calculated in Fig. 1F for EYFP–NLS-β-actin are fitted to the data in Fig. S1A). To ensure that transfection with supervillin fragment predominately affected the nuclear rather than the cytoplasmic actin pool, we performed FRAP assays on diffuse wild-type EYFP–β-actin in the cytoplasm (Fig. S1C). As previously reported, diffuse nuclear and cytoplasmic actin populations showed similar recovery kinetics (Ho et al., 2013; Johnson et al., 2013; McDonald et al., 2006). Importantly, unlike the nucleus (Fig. S1A), co-transfection with the mCherry–supervillin fragment and the formation of nuclear actin filaments had no noticeable effect on wild-type EYFP–β-actin in the cytoplasm (Fig. S1C). These results agree with previous FRAP studies on nuclear actin following treatment with actin-polymerizing drugs (McDonald et al., 2006). The FRAP data support a model wherein the formation of stable nuclear actin filaments decreases the mobility of the remaining, non-filamentous actin in the nucleus, without significantly affecting the cytoplasmic pool of actin.

This model presumes that nuclear actin filaments incorporate endogenous actin. To investigate this possibility, immunoprecipitation assays were performed with an antibody specific to endogenous β-actin (antibodies validated in Fig. S1D) on extracts from COS7 cells expressing EGFP (control), V163M-α-actin–GFP or EYFP–NLS-β-actin. Blots probed for β-actin or GFP (Fig. 2A) demonstrated that endogenous β-actin associates with both exogenous V163M-α-actin–GFP and EYFP–NLS-β-actin. To establish that endogenous actin is directly incorporated into nuclear actin filaments, cells were transfected, fixed with ethanol to expose the actin epitope buried in filaments, and stained with an antibody that preferentially recognizes endogenous actin but not exogenous fluorescent actin (Fig. S1D,E). Fig. S1E shows the presence of endogenous actin in nuclear actin filaments formed by V163M-α-actin–GFP or EYFP–NLS-β-actin, establishing that endogenous actin directly incorporates into nuclear actin filaments. Furthermore, because phalloidin staining is highly specific to actin, phalloidin staining in supervillin-transfected cells (Fig. 1B) can only result from the inclusion of endogenous β-actin into nuclear actin filaments. Indeed, co-transfecting cells with wild-type EYFP–β-actin, which does not form nuclear actin filaments when expressed alone, and the mCherry–supervillin fragment showed that exogenous β-actin is also readily incorporated into nuclear actin filaments (Fig. S1B).

Nuclear actin filaments decrease the concentration of non-filamentous actin in the nucleus

One explanation for the results above is that nuclear actin filaments increase nuclear actin polymerization and thus, sequester and decrease the concentration of non-filamentous actin in the nucleus. We confirmed this possibility by performing molecular brightness (aggregation) analysis. This fluorescence correlation spectroscopy method distinguishes the brightness of a particle from the number of particles in a given volume and, therefore, measures the degree of protein aggregation (Berland et al., 1995; Chen et al., 2003; Digman et al., 2008). Diffuse areas of fluorescence in nuclei expressing EGFP–NLS alone (as an ideal monomer control), EYFP–NLS-β-actin (both nuclear actin filament positive and negative), and EGFP–β-actin in mCherry–supervillin fragment co-expressing nuclei were analyzed (Fig. 2B). We found that EGFP–NLS and EYFP–NLS-β-actin (nuclear actin filament negative) behaved predominantly as monomers; however, EYFP–NLS-β-actin (nuclear actin filament positive) and EGFP–β-actin in supervillin-fragment-containing nuclei exhibited significantly increased molecular brightness. Thus, EYFP–β-actin in the nucleus behaves primarily as a monomer (as compared to EGFP) and exogenous β-actin in nuclei with nuclear actin filaments exhibits an overall increased polymerization state. We also performed 100,000 ***g*** spins on extracts from purified nuclei expressing EYFP–NLS-β-actin, V163M-α-actin–GFP or EGFP, based on the prior demonstration that polymerized actin is found in the pellet (Brotschi et al., 1978). Sedimentation assays show that the majority of nuclear actin remains in the soluble fraction. Furthermore, actin is enriched in the pellet fraction in nuclei containing actin filaments as compared to in EGFP-transfected cells (Fig. 2C). These data support the notion that pathogenic formation of nuclear actin filaments increases the polymerization and sequestration of nuclear actin.

We then investigated whether formation of nuclear actin filaments decreased the monomeric actin pool in the nucleus. Transfected cells were fixed with formaldehyde, which preserves the filamentous actin structure and limits access to the actin epitopes buried within actin filaments (Gonsior et al., 1999), and stained with an antibody that recognizes endogenous non-filamentous nuclear actin (Cisterna et al., 2006; Sacco-Bubulya and Spector, 2002). Because this antibody recognizes actin filaments poorly after formaldehyde fixation, the nuclear fluorescence results from binding to non-filamentous actin. Fluorescence intensity quantification showed that cells with nuclear actin filaments had less non-filamentous actin staining in the nucleus (Fig. 2D). These data establish that formation of persistent nuclear actin filaments increases nuclear actin polymerization (Figs 1E,F, 2B–D; Fig. S1A–C) and sequesters endogenous actin (Figs 1A–D, 2A; Fig. S1E), thereby decreasing the pool of monomeric actin in the nucleus.

Nuclear actin filament formation decreases general transcription and proliferation

To quantify the overarching effects of forming persistent nuclear actin filaments and sequestering nuclear actin, COS7 cells were treated with BrU or BrdU, nucleotide analogs that preferentially incorporate into mRNA or DNA, respectively (Lin et al., 2008). Nuclei with actin filaments showed a decrease in BrU incorporation, indicating that the formation of nuclear actin filaments coincides with reduced levels of global transcription (Fig. 3A). Importantly, both the polymerization-resistant actin mutant NLS-R62D-β-actin and wild-type actin, which increase cytoplasmic actin levels, had no effect. Co-transfection with the mCherry–supervillin fragment to induce nuclear actin filaments and either wild-type or EYFP-NLS-R62D-β-actin showed that increasing nuclear but not cytoplasmic levels of monomeric actin was able to rescue the effects of nuclear actin filaments on transcription (Fig. 3B). This suggests that the reduction in transcription is specific to the increase in nuclear actin polymerization. This finding is consistent with work by Dopie et al. (Dopie et al., 2012), which showed that knockdown of the actin import factor (Imp9, also known as IPO9) decreased nuclear actin levels and, correspondingly, general transcription. Our results are also consistent with other reports that have found that depleting or polymerizing nuclear actin leads to decreased general transcription (Daugherty et al., 2014; Dopie et al., 2012; Spencer et al., 2011).

We next used a SRF-dependent luciferase construct to determine whether the residual transcription activity in these cells could be from genes that are upregulated upon nuclear actin filament

Journal of Cell Science

Journal of Cell Science (2016) 129, 3412-3425 doi:10.1242/jcs.195867

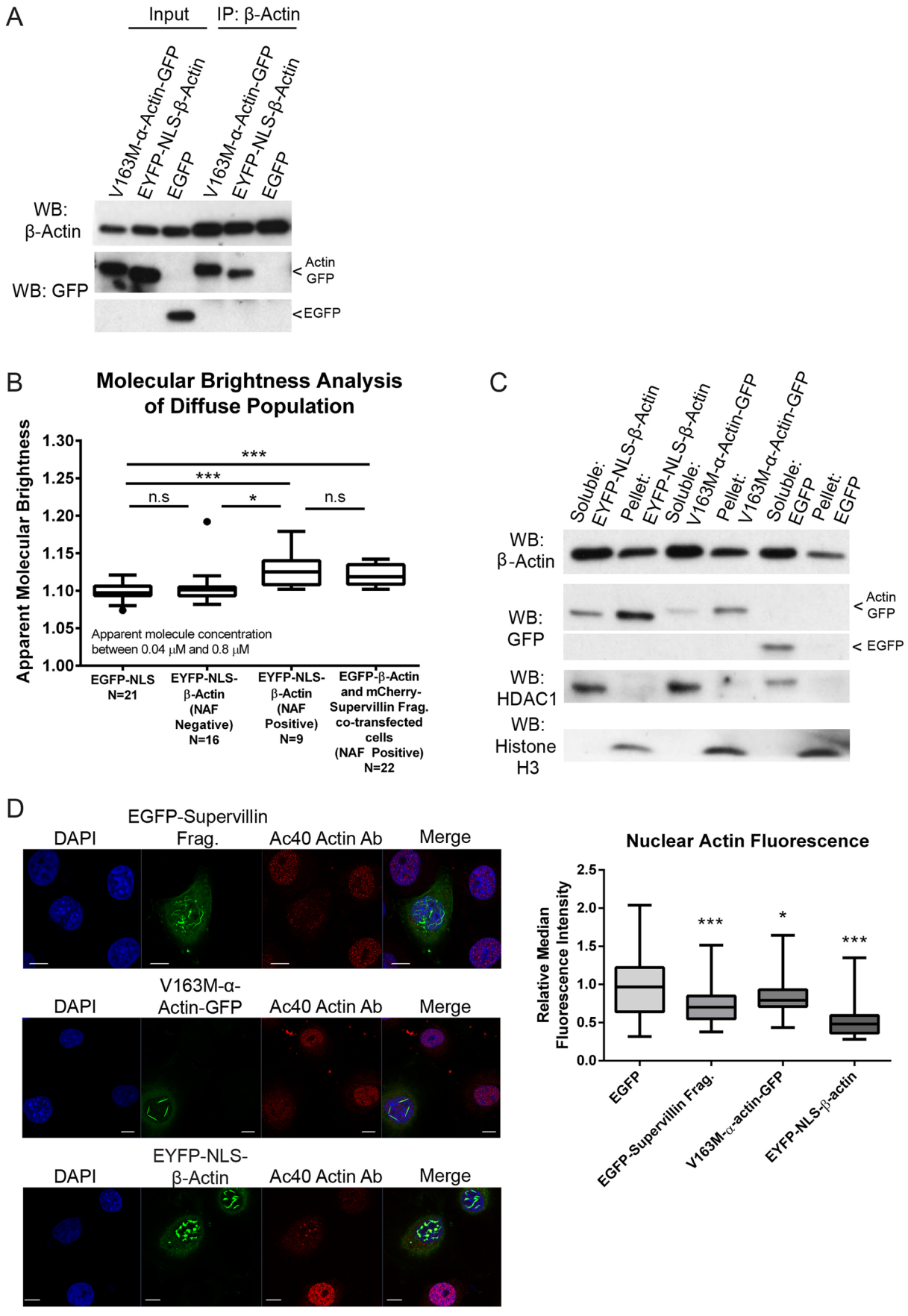

Fig. 2. See next page for legend.

Journal of Cell Science

Journal of Cell Science (2016) 129, 3412-3425 doi:10.1242/jcs.195867

Fig. 2. Nuclear actin filaments incorporate and sequester nuclear actin. (A) Co-immunoprecipitation assay of HeLa cells transfected with the indicated constructs and immunoprecipitated (IP) with an antibody against endogenous β-actin. Immunoblotting with antibodies to β-actin and GFP demonstrated the interaction of the exogenous and endogenous actin. (B) Tukey box plot (the box represents the 25–75th percentiles, and the median is indicated; the whiskers show the 1.5 times the interquartile distance; dots represent outliers) showing the molecular brightness analysis performed on nuclei expressing EGFP–NLS (ideal monomer control), EYFP–NLS-β-actin [nuclear actin filament (NAF) negative], EYFP–NLS-β-actin (NAF positive), and EGFP–β-actin in supervillin fragment co-expressing cells. Note the increased brightness measurements in nuclei with nuclear actin filaments. *P<0.05; ***P<0.001; n.s, not significant (one-way ANOVA). (C) 100,000 ***g*** sedimentation assay of purified nuclear extracts prepared from cells expressing EYFP–NLS-β-actin, V163M-α-actin–GFP or EGFP. HDAC1 and histone H3 were used as loading controls. Note the relative enrichment of endogenous actin in the pellet fraction of nuclei with nuclear actin filaments versus EGFP alone. WB, western blotting. (D) COS7 cells were transfected with the indicated constructs fixed with formaldehyde and stained with anti-actin antibodies (AC40). Fluorescence quantification, presented in a box plot, with the whiskers representing minimum to maximum values, shows a reduction in endogenous non-filamentous actin levels with nuclear actin filament formation. n>30. *P<0.05; ***P<0.001 (one-way ANOVA). Fluorescence intensity was normalized to non-transfected cells in each frame. Scale bars: 10 µm.

formation. Previous reports have shown that nuclear actin filaments sequester monomeric nuclear actin and activate the MAL–SRF pathway (Baarlink et al., 2013; Ho et al., 2013; Kokai et al., 2014; Vartiainen et al., 2007). Similarly, we find EYFP–NLS-S14C-β-actin and EGFP–supervillin fragment expression both increase induction of the SRF-dependent reporter (Fig. S2A). These data suggest that nuclear actin filament formation has an inhibitory effect on general transcription, but this does not preclude specific gene stimulation by transcription factors that are activated by the depletion of nuclear actin.

Analysis of BrdU incorporation and cell number counts consistently demonstrated that proliferation of nuclear actin filament positive cells is reduced >50% (Fig. 3C; Fig. S2B). However, there was no increase in apoptosis in cells with nuclear actin filaments as determined by a TUNEL assay (Fig. S2C). Therefore, the global decreases in transcription and proliferation in cells with nuclear actin filaments likely underlie the importance of maintaining a monomeric pool of nuclear actin.

Nuclear actin filament formation alters RNAPII localization and dynamics

To determine whether the decrease in general transcription was related to changes in RNAPII, we assessed how formation of nuclear actin filaments affects RNAPII localization and dynamics. Structured illumination microscopy (SIM) on cells stained for active RNAPII revealed relatively evenly distributed RNAPII in small transcription factories throughout the nucleus in non-transfected cells (Fig. 4A). However, the presence of stable nuclear actin filaments coincided with the appearance of unusually large factories or clusters (Fig. 4B–D). We noted a significant difference in mean transcription factory size and an increase in the maximum range compared to nuclei without actin filaments (Fig. 4E). Furthermore, co-transfecting cells with the mCherry–supervillin fragment to induce nuclear filaments and EYFP–NLS-R62D-β-actin to increase nuclear actin levels restored transcription factory size to that of non-transfected cells (Fig. 4E; Fig. S3A). We generated a COS7 cell line stably expressing the large subunit of RNAPII conjugated to GFP to determine whether altering nuclear actin polymerization affects RNAPII dynamics. These cells exhibit many small (<0.5 µm), and a limited number of medium sized (0.5–1 µm), transcription factories (Fig. 4F). GFP–RNAPII cells transfected with the mCherry–supervillin fragment, in contrast, have small and large (>1 µm) factories. FRAP studies on small factories in control cells and cells containing nuclear actin filaments showed similar recoveries (Fig. 4F). However, FRAP studies on large factories in actin-filament-containing nuclei showed that they are consistently less dynamic than small factories (Fig. 4F; Table S1B). These data suggest a role for nuclear actin in regulating transcription factory dynamics.

The temporal relationship between transcription factory size and nuclear actin polymerization was investigated by transfecting COS7 cells with the EGFP–supervillin fragment (Fig. S3B) or EYFP–NLS-β-actin (Fig. S3C). Cells were fixed over 32 h, stained for RNAPII, and RNAPII clustering was correlated with construct expression (Fig. S3B–D). As construct expression increased with time so did the percentage of transfected cells with visible nuclear actin filaments. This experiment demonstrated the presence of RNAPII clustering in transfected cells before the formation of nuclear actin filaments (Fig. S3B–D). Furthermore, we found RNAPII clusters in no more than 4% and 1% of cells with cytoplasmic expression of the EGFP–supervillin fragment or EYFP–NLS-β-actin, respectively. This strongly suggests that RNAPII clustering is not due to changes in cytoplasmic actin. Additionally, treatment with the actin-depolymerizing drug latrunculin B or the myosin II inhibitor blebbistatin did not have an effect on RNAPII localization (Fig. S3E). The major implication of these data is that polymerizing nuclear actin increases RNAPII clustering, but filaments, per se, are not needed to cluster RNAPII.

The effect of nuclear actin filaments on gene transcription, *in vivo*, was investigated next using the U2OS-263 system (Fig. 4G). U2OS-263 cells have 200 repeats of an inducible gene cassette stably integrated at a single locus (Darzacq et al., 2007). Each repeat encodes an mRNA with a 24-nucleotide stem-loop repeat in its 3′ untranslated region. U2OS-263 cells were co-transfected with MS2–GFP, an RNA-stem-loop-binding protein, to track transcription, and the mCherry–supervillin fragment to form nuclear actin filaments. Upon induction, the gene cassette is transcribed, and MS2–GFP accumulates at the transcribed cassette and serves as a direct measure of transcript synthesis. FRAP assays were performed to assess whether the rates of transcription of the cassette differ in control cells and cells containing nuclear actin filaments. Quantification of the accumulation of MS2–GFP fluorescence after bleaching showed reduced MS2 fluorescence recovery in nuclei expressing the mCherry–supervillin fragment as compared to nuclei without actin filaments (Fig. 4G; Table S1C). These results are consistent with a slower rate of transcription (Darzacq et al., 2007).

Nuclear actin filament formation reduces the interaction of actin with RNAPII and RNAPII gene recruitment

The results above suggested that nuclear actin filaments impact RNAPII clustering, perhaps by altering the actin–RNAPII interaction. We investigated this possibility by performing GFP pulldowns on cells expressing polymerization-promoting (S14C) or polymerization-resistant (R62D) EYFP–NLS-β-actin mutants (Posern et al., 2002). Western blot analyses showed a higher ratio of RNAPII to EYFP in pulldowns of cells expressing EYFP–NLS-R62D-β-actin compared to cells expressing EGFP or EYFP–NLS-S14C-β-actin (Fig. 5A). This preferred association of RNAPII with a polymerization-resistant β-actin is in agreement with the poor colocalization between nuclear actin filaments and RNAPII (Fig. 4A), as well as between actin polymers and RNAPII (Belin et al., 2013). Furthermore, immunoprecipitation experiments showed a reduced association between RNAPII and β-actin in cells with nuclear actin filaments versus EGFP-transfected control

Journal of Cell Science

Journal of Cell Science (2016) 129, 3412-3425 doi:10.1242/jcs.195867

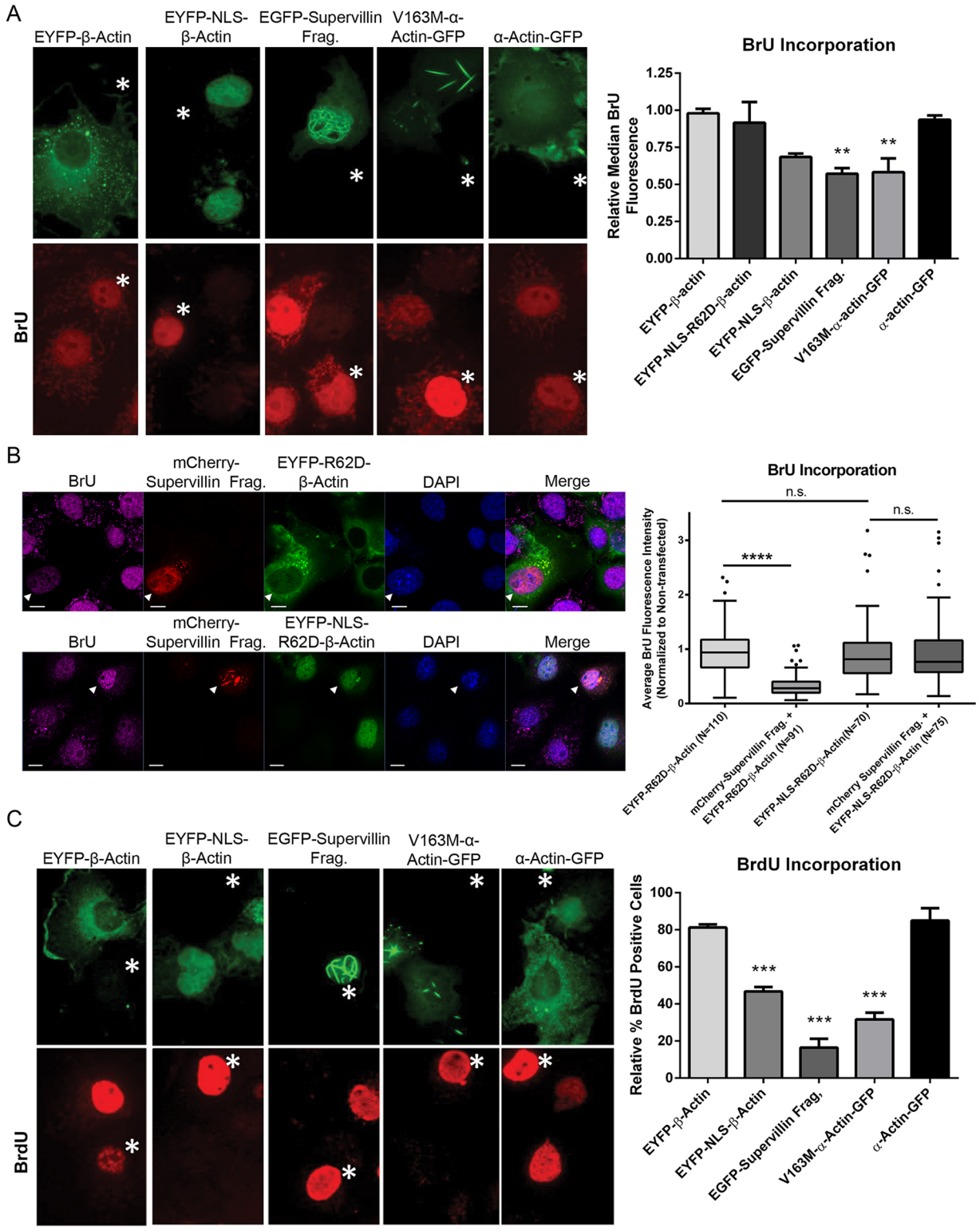

Fig. 3. Nuclear actin filament formation inhibits transcription and proliferation. (A) COS7 cells transfected as shown (green) were treated with 2 mM BrU, stained for BrU incorporation (red) and normalized to non-transfected cells (asterisks). Quantification of BrU fluorescence is shown on the right. Fluorescence intensity was normalized to non-transfected cells in each frame. Results are mean±s.e.m. (n=3, >300 cells/group). **P<0.01 (one-way ANOVA). (B) COS7 cells co-transfected with the mCherry–supervillin fragment and either wild-type EYFP–R62D-β-actin or EYFP–NLS-R62D-β-actin for 48 h then treated with BrU as in A. Arrowheads denote nuclei with filaments. Quantification of the fluorescence intensity shows increasing R62D-actin levels in the nucleus, but not in the cytoplasm, is able to restore transcription levels. Fluorescence intensity was normalized to non-transfected cells in each frame (Tukey box plot indicates the 25–75th percentiles, and the median; the whiskers show 1.5 times the interquartile distance; dots represent outliers). ****P<0.0001; n.s., not significant (one-way ANOVA). (C) Transfected COS7 cells were treated with 10 µM BrdU for 5 h, stained for BrdU incorporation (red), and normalized to non-transfected cells (asterisks). Quantification of BrU fluorescence is shown on the right. Fluorescence intensity was normalized to non-transfected cells in each frame. Results are mean± s.e.m. (n=5, >400 cells/group). ***P<0.001 (one-way ANOVA).

Journal of Cell Science

Journal of Cell Science (2016) 129, 3412-3425 doi:10.1242/jcs.195867

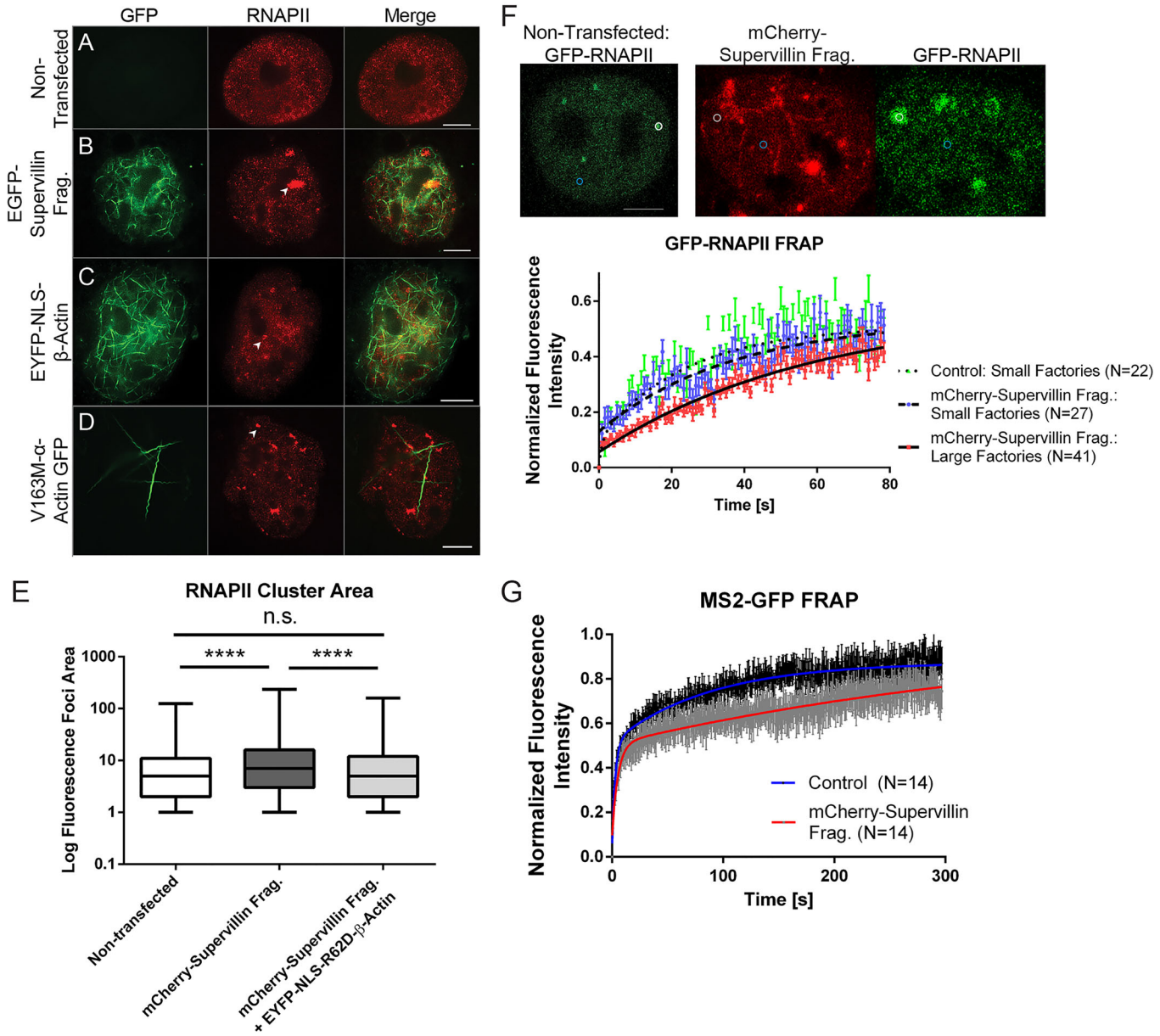

Fig. 4. Nuclear actin filament formation impairs RNAPII localization and dynamics. Structured illumination microscopy of (A) control and cells transfected with (B) the EGFP–supervillin fragment, (C) EYFP–NLS-β-actin, (D) V163M-α-actin–GFP, and stained with anti-phospho-RNAPII (4H8) antibody. White arrowheads show large RNAPII clusters in transfected cells. Scale bars: 5 µm. (E) RNAPII foci area (# square pixels) in non-transfected, mCherry–supervillin-fragment-transfected, and cells co-transfected with the mCherry–supervillin fragment and EYFP–NLS-R62D-β-actin was graphed to log scale using a box plot (the box represents the 25–75th percentiles, and the median is indicated; the whiskers show the min. and max. values); >2500 foci were mapped in each group. Demonstrative images are shown in Fig. S3A. (F) FRAP analyses of RNAPII dynamics of COS7 cells stably expressing GFP-RNAPII. FRAP curves show data points as mean± s.e.m. and recovery lines of best fit. FRAP kinetics are listed in Table S1B. FRAP analyses were performed on small RNAPII transcription factories in control cells (green data points, dotted line) or on cells co-transfected with the mCherry–supervillin fragment that exhibit small transcription factories (blue data points, dashed line) and large factories (red data points, solid line). Large factories exhibited a slower fluorescence recovery. In each micrograph, small foci are marked with blue circles, whereas medium (control nuclei) and large foci (nuclear-actin-filament-positive nuclei) are marked with white circles. Scale bars: 5 µm. (G) U2OS-263 cells co-transfected with MS2–GFP and the mCherry–supervillin fragment. FRAP analysis (mean±s.e.m.) of cells transfected with the mCherry–supervillin fragment (red and gray) show decreased MS2–GFP fluorescence recovery as compared to control cells (blue and black). FRAP kinetics are listed in Table S1C.

cells (Fig. 5B). These data further support the notion that the incorporation of endogenous actin into nuclear actin filaments depletes the available non-polymerized nuclear actin pool, thereby reducing the actin–RNAPII interaction.

We have previously shown that the actin–RNAPII complex is specifically recruited to the MHCIITA (also known as CIITA) promoter upon induction with interferon-γ (Hofmann et al., 2004). Therefore, we asked whether the recruitment of RNAPII to the MHCIITA promoter is impaired by sequestering nuclear actin. ChIP-qPCR assays showed significant decreases in RNAPII recruitment in cells with nuclear actin filaments compared to cells expressing EGFP alone (Fig. 5C). Reporter gene experiments showed that induction of the MHCIITA promoter with interferon-γ was significantly reduced in cells with

Journal of Cell Science

Journal of Cell Science (2016) 129, 3412-3425 doi:10.1242/jcs.195867

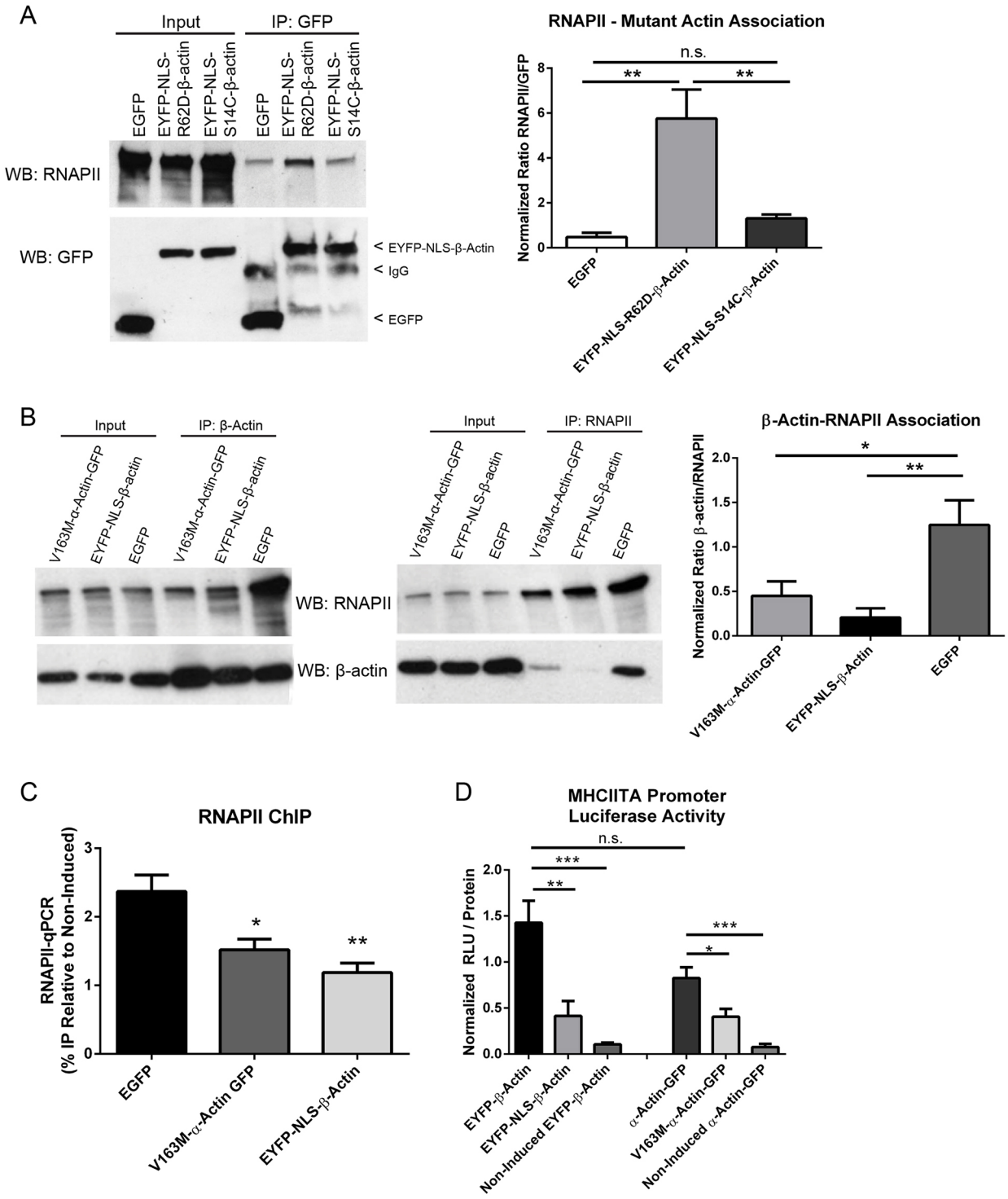

Fig. 5. Nuclear actin filament formation reduces the interaction of actin with RNAPII and RNAPII gene recruitment. (A) GFP immunoprecipitation (IP) assay on HeLa cells transfected with EGFP or EYFP–NLS-β-actin with the S14C (polymerization promoting) or R62D (polymerization resistant) mutation. WB, western blotting. Quantification of the ratio of RNAPII levels to GFP levels shows that RNAPII (H14 antibody) associates better with the polymerization-resistant (R62D) mutant. Data were normalized to the ratio of RNAPII and GFP in the input lanes. Results are mean±s.e.m. (n=4). **P<0.01 (one-way ANOVA). (B) Co-immunoprecipitation assay of HeLa cells transfected with GFP or constructs that led to the formation of nuclear actin filaments and immunoprecipitated with antibodies to endogenous β-actin (left) or RNAPII (4H8 antibody, right) and blotted for RNAPII (H14 antibody) and β-actin. The quantification of β-actin to RNAPII levels shows a reduced interaction between endogenous β-actin and RNAPII in cells containing nuclear actin filament as compared to cells with EGFP alone. Data were normalized to the ratio of RNAPII and GFP in the input lanes. Results are mean±s.e.m. (n=4). *P<0.05; **P<0.01 (one-way ANOVA). (C) ChIP-qPCR analysis of the recruitment of RNAPII to the activated MHCIITA promoter in cells containing nuclear actin filaments. Data were calculated as a percentage of input and normalized to enrichment in non-induced cells. Results are mean±s.e.m. (n=4). *P<0.05; **P<0.01 (one-way ANOVA). (D) Luciferase assay of the MHCIITA promoter as a measure of gene activation in cells expressing actin controls or in cells with nuclear actin filaments. Relative luciferase units per µg of protein in each lysate was calculated and normalized to cells transfected with only the MHCIITA promoter luciferase construct. Results are mean± s.e.m. (n=6). *P<0.05; **P<0.01; ***P<0.001; n.s., not significant (t-test).

Journal of Cell Science

Journal of Cell Science (2016) 129, 3412-3425 doi:10.1242/jcs.195867

nuclear actin filaments (Fig. 5D), in agreement with the effects on general transcription (Fig. 3A). We complemented these studies by directly inhibiting RNAPII with α-amanitin or 5,6-dichloro-1-b-dribofuranosylbenzimidazole (DRB), chemical inhibitors of RNAPII that result in the formation of enlarged transcription factories (Bregman et al., 1995) (Fig. S4A). Although some actin still associates with these enlarged factories (Fig. S4B), co-immunoprecipitation experiments revealed an overall decrease in the association between RNAPII and actin (Fig. S4C). Whereas the large transcription factories formed by direct RNAPII inhibition are morphologically distinct from RNAPII clusters induced by nuclear actin filaments (note SC-35 colocalization with RNAPII in Fig. S4A but not Fig. S4D), these results closely parallel the effects of nuclear actin filaments on RNAPII. They also support the importance of the actin–RNAPII association and further affirm the idea that nuclear actin might be a dynamic regulator of RNAPII localization.

Crosslinking or polymerizing nuclear actin inhibits mRNA transcription *in vitro*

We next determined whether reducing the monomeric concentration of actin, by crosslinking or polymerizing actin, is sufficient to inhibit transcription *in vitro*. First, we pre-incubated HeLa nuclear extracts with vehicle or the purified actin-crosslinking domain (ACD) of *V. cholera* MARTX. ACD toxin catalyzes inter-molecular amide bond formation between actin monomers, covalently crosslinking monomeric actin (Kudryashov et al., 2008). Western blots of ACD-treated nuclear extracts showed a ladder of actin crosslinked into oligomers of increasing molecular weights and a concomitant decrease in the amount of non-crosslinked actin (Fig. 6A). *In vitro* transcription assays on nuclear extracts incubated with ACD showed significantly reduced levels of transcription compared to vehicle (Fig. 6B). Immunoprecipitation of RNAPII showed that the amount of uncrosslinked actin bound to RNAPII is decreased following ACD treatment and RNAPII binds crosslinked actin poorly if at all (Fig. 6C). Second, we performed *in vitro* transcription assays in HeLa nuclear extracts pre-incubated with phalloidin. Sedimentation assays performed on purified HeLa nuclear extract incubated with phalloidin showed a dramatic shift from the soluble to the insoluble pool of nuclear actin (Fig. 6D). Furthermore, extracts pre-treated with 10 μM phalloidin exhibited significantly decreased rates of *in vitro* transcription (Fig. 6E). Correspondingly, we found adding phalloidin decreased the amount of actin co-immunoprecipitated with RNAPII (Fig. 6F). Taken together, these *in vitro* effects parallel those of forming nuclear actin filaments in cells and demonstrate that oligomeric actin structures or polymerized actin decreases the amount of native actin available to interact with RNAPII. This decreased association of actin with RNAPII coincides with a decrease in transcription independent of nuclear actin filament formation.

DISCUSSION

It is now established that actin is an abundant nuclear protein (de Lanerolle and Serebryannyy, 2011; Gettemans et al., 2005; Grosse and Vartiainen, 2013). However, the form and functions of nuclear actin in normal mammalian nuclei remain controversial. Taking advantage of an actin mutation that promotes nuclear actin filament formation and disease, along with approaches to induce nuclear actin filaments both in cells and *in vitro*, we show that forming nuclear actin filaments inhibits transcription by RNAPII. Formation of nuclear actin filaments sequesters a pool of non-polymeric actin required for the proper localization and activation of RNAPII. Overall, our data appear to rationalize the general absence of stable actin filaments in mammalian somatic nuclei. Although our study aimed to understand the role of persistent or stable nuclear actin filaments on transcription, recent studies have reported that nuclear actin polymers and filaments can be transiently induced by specific stimuli (Baarlink et al., 2013; Belin et al., 2013, 2015; McDonald et al., 2006; Plessner et al., 2015). Thus, these studies, together with our own, suggest the exciting possibility that nuclear actin might exist in a dynamic equilibrium between transiently formed polymers and monomers that locally regulate transcription.

Our findings are consistent with previous work demonstrating a role for nuclear actin in mRNA transcription (Egly et al., 1984; Hofmann et al., 2004; Scheer et al., 1984). We find that sequestering actin in nuclear actin filaments (Fig. 2) correlates with reduced MHCIITA promoter recruitment (Fig. 5C) and lower rates of gene transcription (Figs 3A,B, 4G and 5D). In agreement, RNAPII preferentially interacts with the non-polymerizing R62D-β-actin mutant rather than the polymerization-promoting S14C-β-actin mutant (Fig. 5A). Moreover, the actin–RNAPII interaction is impaired in the presence of nuclear actin filaments (Fig. 5B), actin polymerization by phalloidin, and actin crosslinking (Fig. 6). Notably, we find expression of nuclear localized R62D-β-actin, but not cytoplasmic R62D-β-actin, is able to restore transcription in nuclei with filaments (Fig. 3B). Similarly, depleting nuclear actin through changes in growth factors or extracellular molecules has been reported to inhibit RNAPII activity, and this inhibition can be rescued by expressing NLS-R62D-β-actin (Spencer et al., 2011). These data, which support the notion that monomeric actin is important in maintaining transcription, are consistent with the previous demonstration that monomeric nuclear actin interacts with chromatin remodeling complexes (Kapoor and Shen, 2014; Serebryannyy et al., 2016) and the transcription factor MAL (Vartiainen et al., 2007).

Our *in vitro* transcription assays similarly demonstrate that polymerizing actin represses RNAPII (Fig. 6). Importantly, these assays investigate the effects of polymerizing and crosslinking actin independently of nuclear actin filament formation, changes in nuclear architecture or cytoplasmic actin. Crosslinked actin does not interact with RNAPII and less actin associates with RNAPII when actin is polymerized with phalloidin (Fig. 6). It is telling that crosslinking actin with ACD or polymerizing actin with phalloidin led to significant decreases in mRNA transcription (Fig. 6B,E). Similarly, Egly et al. have reported that adding actin to *in vitro* transcription assays stimulates mRNA transcription, but actin pre-treated with phalloidin abolishes the increase seen with actin alone, strongly suggesting that polymerized actin inhibits transcription (Egly et al., 1984). Because treatments that increase nuclear actin polymerization inhibit RNAPII activity, these results denote that nuclear actin monomers or highly dynamic polymers facilitate transcription.

One of our most striking observations was the reorganization of RNAPII into larger clusters in nuclei with actin filaments (Fig. 4A–F). Is this due to the effect of nuclear actin filaments on the availability of monomeric actin in the nucleus or to a secondary effect? Our data argue in favor of the former. Co-expressing NLS-R62D-β-actin, to increase the levels of monomeric nuclear actin, with the mCherry–supervillin fragment to induce filaments, decreased the size of RNAPII clusters (Fig. 4B; Fig. S3A), strongly suggesting a role for monomeric actin in transcription. Furthermore, RNAPII clusters induced by nuclear actin filaments exhibit multiple similarities to those found with direct RNAPII inhibition (Bregman et al., 1995), including a decrease in the actin–RNAPII interaction and changes in the organization of RNAPII (Fig. S4). Interestingly, direct pharmacological inhibition of

Journal of Cell Science

Journal of Cell Science (2016) 129, 3412-3425 doi:10.1242/jcs.195867

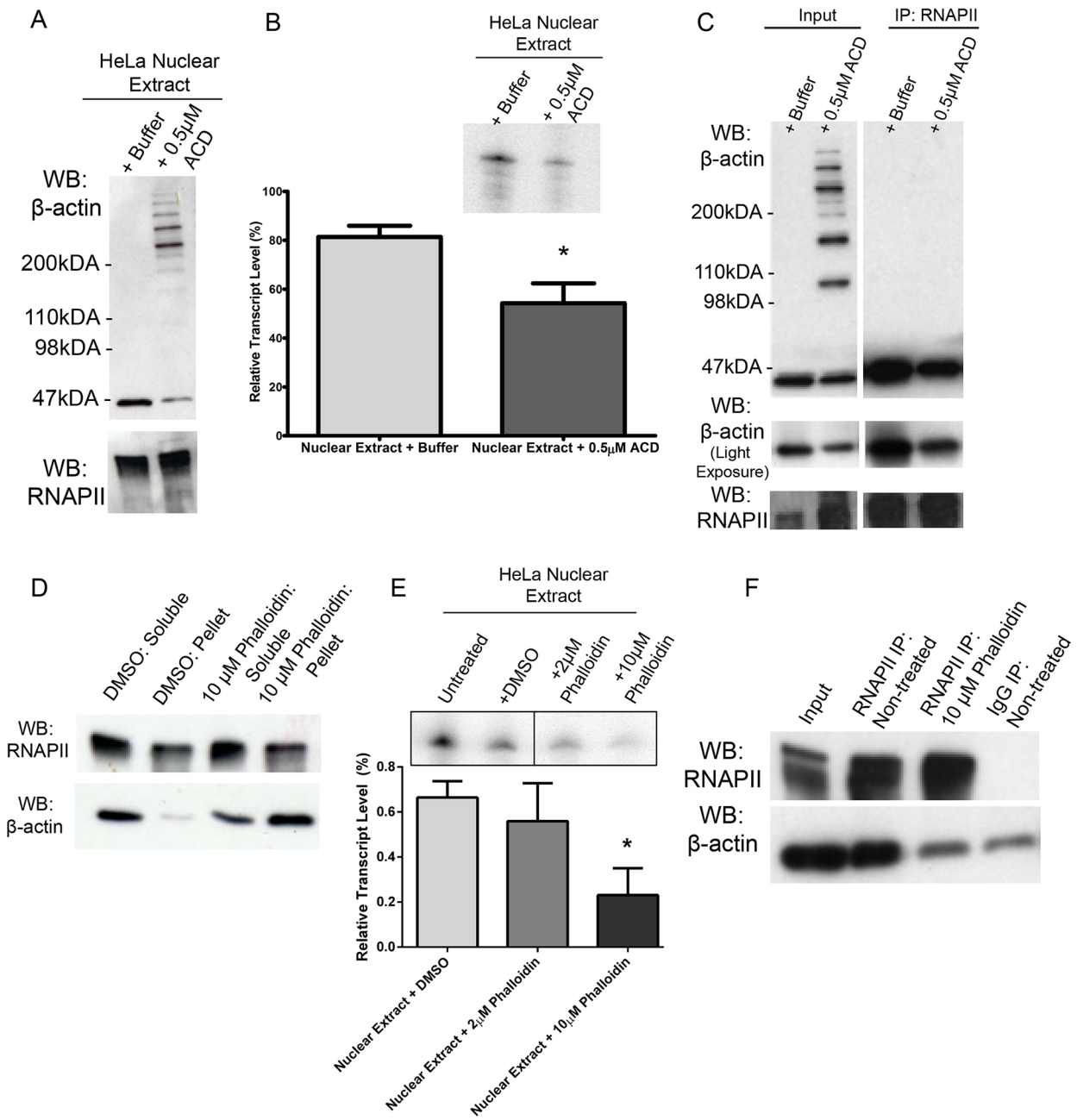

Fig. 6. Sequestering nuclear actin inhibits transcription *in vitro*. (A) Representative immunoblot of HeLa nuclear extract pre-incubated with buffer or 0.5 µM ACD to crosslink nuclear actin, and probed with antibodies to β-actin (top) and RNAPII (bottom). WB, western blotting. (B) Graph of ^{32}[P]-labeled RNA transcripts from an adenovirus major late promoter cassette incubated with HeLa nuclear extract pre-treated with buffer or 0.5 µM ACD. A representative autoradiograph is shown. Quantification of transcript band density normalized to HeLa nuclear extract alone shows a significant decrease in transcription in ACD-treated extracts. Results are mean±s.e.m. (n=5). *P<0.05 (t-test). (C) Immunoprecipitation (IP) of RNAPII (4H8 antibody) from HeLa cell nuclear extract treated with buffer or ACD and probed with β-actin (top) and RNAPII (H14) antibody (bottom). Note the lack of high-molecular-mass actin species in the ACD-treated immunoprecipitate and lower levels of associated monomeric β-actin. (D) 100,000 ***g*** sedimentation assays of purified HeLa nuclear extract pre-treated with DMSO or 10 µM phalloidin. (E) Graph of ^{32}[P]-labeled RNA transcripts as in B pre-treated with DMSO, 2 µM, or 10 µM phalloidin. A representative autoradiograph is shown. Quantification of transcript band density, normalized to untreated HeLa nuclear extract, shows significant decreases in transcription in extracts treated with 10 µM phalloidin. Results are mean±s.e.m. (n=3). *P<0.05 (one-way ANOVA). (F) Immunoprecipitation of RNAPII (4H8 antibody) from HeLa nuclear extract after treatment with vehicle or 10 µM phalloidin. Western blots were probed with RNAPII (H14) antibody (top) and β-actin (bottom).

RNAPII in *Xenopus* oocyte nuclei increases nuclear actin polymerization (Scheer et al., 1984), and nuclear actin polymerization might be necessary for RNAPII interchromatin granule clusters formed during transcription inhibition in mammalian cells (Wang et al., 2006). Another possibility is that the constructs used to polymerize nuclear actin alter actin polymerization in the cytoplasm. However, RNAPII clustering is very rare when these constructs are only expressed in the cytoplasm, and depolymerizing the actin cytoskeleton or inhibiting myosin II did not change the effect of nuclear actin filaments on RNAPII clustering or transcription (Figs 3, 4; Fig. S3). Thus, the reorganization of RNAPII into large factories in nuclei with actin

Journal of Cell Science

Journal of Cell Science (2016) 129, 3412-3425 doi:10.1242/jcs.195867

filaments is likely due to the polymerization and subsequent sequestering of nuclear actin, not cytoplasmic influences or the filaments themselves.

Taken together, our data point to a model in which a dynamic pool of nuclear actin affects the localization and dynamics of active RNAPII, perhaps bound to other actin-binding proteins such as cofilin (Dopie et al., 2012; Obrdlik and Percipalle, 2011). They suggest a model in which polymerizing nuclear actin sequesters and decreases the monomeric pool of actin. This, in turn, attenuates the actin–RNAPII interaction and RNAPII activity and decreases transcription and proliferation (Figs 3, 5 and 6). This model is consistent with studies in which injecting actin antibodies or depleting nuclear actin inhibited transcription (Hofmann et al., 2004; Rungger et al., 1979; Scheer et al., 1984; Spencer et al., 2011). In support of this idea, monomeric actin (Posern et al., 2002; Vartiainen et al., 2007) and transient actin filaments (Baarlink et al., 2013; Plessner and Grosse, 2015) have been implicated in signal transduction whereas stable nuclear actin filaments are associated with pathologies (Domazetovska et al., 2007b; Munsie et al., 2011; Stenzel et al., 2015). Because actin filament formation is related to the monomer concentration (Pollard and Cooper, 2009), regulating the concentration of nuclear actin might be one mechanism for preventing the formation of persistent filaments and avoiding their negative effects.

This model is distinct from models describing cytoplasmic actin, which are dominated by the polymerization of actin into filaments that interact with myosins to generate force (Pollard and Cooper, 2009). However, actin evolved long before the first myosin (Goodson and Hawse, 2002; Hofmann et al., 2009; Pollard and Cooper, 2009) and actin must have had essential, conserved functions that predated myosin-mediated force production. Importantly, our data suggest roles for nuclear actin that are independent of its ability to form canonical filaments. It is tempting to speculate that a pool of non-polymerized actin might be able to interact more adroitly with multiple binding partners than filamentous actin. Although this possibility is intriguing, additional experiments are needed to fully understand the role of actin polymerization on the nucleus.

MATERIALS AND METHODS

Cell culture and antibodies

COS7 and HeLa cells were obtained from the ATCC and cultured in Dulbecco's modified Eagle's medium (DMEM; Corning) supplemented with 1% penicillin–streptomycin and 10% fetal bovine serum (Invitrogen).

Primary antibodies were purchased as shown: RNAPII antibodies, H5, H14 (western blotting, 1:5000) (Covance), 4H8 (immunofluorescence, 1:150; western blotting, 1:5000; immunoprecipitation, 5 µg) (Abcam and Active Motif); β-actin antibodies Ac-15 (immunofluorescence, 1:200; western blotting, 1:10,000; immunoprecipitation, 5 µg) and Ac-40 (immunofluorescence, 1:100; western blotting, 1:1000) (Sigma-Aldrich) and pan-actin C4 (immunofluorescence, 1:100; western blotting, 1:5000) (EMD Millipore); non-specific IgG (immunoprecipitation, 5 µg) (Santa Cruz Biotechnology); BrdU/BrU (immunofluorescence, 1:200) (BU-1, EMD Millipore), GFP (immunoprecipitation, 3 µg) (Abcam) and SC-35 (immunofluorescence, 1:100) (SRp30b, EMD Millipore).

Secondary antibodies (1:100) were used as follows: goat IgGs conjugated to Dylight 488 (Thermo Scientific), Texas Red (Jackson Labs), Cy3 (Jackson Labs) and Cy5 (Jackson Labs), as well as Rhodamine–phalloidin (1:400) (Cytoskeleton Inc.). Mounting medium containing DAPI (Vectashield) was used for immunocytochemistry.

Plasmids and transfections

The following constructs were as previously described: EGFP–supervillin fragment (Wulfkuhle et al., 1999), α-actin–GFP and the V163M mutant (Domazetovska et al., 2007a), the EYFP–NLS-β-actin construct and mutations of it (Chang et al., 2011; Posern et al., 2002), GFP–RNAPII (Sugaya et al., 2000) and the MHCIITA promoter luciferase construct (Hofmann et al., 2004). To generate the mCherry–supervillin fragment, the original construct was cut using EcoRI, purified, and inserted into the pmCherry-C1 vector backbone (Clontech). The U2OS-263 system was used as described (Darzacq et al., 2007).

Cell transfections were carried out using Polyjet (SignaGen), ExtremeGene HD (Roche) or JetPrime (Polyplus) reagents. Transfection conditions were optimized to obtain comparable levels of EGFP between constructs to minimize non-specific effects.

COS7 cells were transfected with the GFP–RNAPII (RPB1) construct and selected with 0.5 µg/ml α-amanitin (Santa Cruz Biotechnology) added directly into the medium. Colonies were selected and grown continually in DMEM supplemented with 0.5 µg/ml α-amanitin. Where indicated, 5,6-dichloro-1-b-dribofuranosylbenzimidazole (DRB, Calbiochem) or α-amanitin was added directly into the medium for 3 h at 100 mM and 10 µg/ml, respectively.

Immunostaining

Cells were plated on glass coverslips >24 h before fixation or transfection. Cells were fixed in 4% paraformaldehyde (PFA) for 10 m permeabilized with 0.3% Triton X-100 (Sigma-Aldrich) in PBS for 7 min. For ethanol fixation, cells were briefly fixed in cold absolute alcohol and washed thoroughly. Cells were washed with PBS and incubated in 2% BSA in PBS for 1 h at room temperature and stained using a humidity chamber. Primary antibody was added for 1 h at room temperature or overnight at 4°C. Cells were washed with PBS and secondary antibody was added for 1 h at room temperature. Cells were washed and mounted using Vectashield containing DAPI.

Microscopy

Confocal images were obtained using a Zeiss LSM 710 confocal microscope at the UIC Confocal Microscopy Facility or at the UCI Laboratory for Fluorescence Dynamics. Images were analyzed using Zeiss Zen software. Structured illumination microscopy was performed using a Nikon N-SIM super resolution microscope through the Nikon Imaging center at Northwestern University.

FRAP imaging

EYFP–NLS-β-actin, EYFP–β-actin and GFP–RNAPII FRAP was performed using a Zeiss LSM 710 confocal microscope with a 63×1.46 NA oil alpha Plan-Apochromat objective. COS7 cells were transfected or pre-treated with the indicated drugs and incubated at 37°C and 5% CO_2 during image acquisition. To perform FRAP, five pre-bleach images were taken before nuclei were bleached in ∼1 µm circles at 100% 488 nm laser power for 25 iterations. Images were collected at 0.5 s for 60–120 s.

MS2–GFP FRAP was performed on U2OS-263 cells co-transfected with the mCherry–supervillin fragment, the doxycycline-sensitive transcriptional activator chimera rTetR and MS2–GFP for 48 h (Darzacq et al., 2007). Images were acquired using a Zeiss LSM 710 confocal microscope with a 40×1.2 NA water alpha Plan-Apochromat objective. Five pre-bleach images were acquired at 256×256 resolution, then MS2 foci were bleached in ∼2 µm circles at 100% 488 nm laser power for 100 iterations. Images were acquired every 600 ms for 500 s.

Fluorescence intensity was normalized to pre-bleach intensity and corrected for non-specific photobleaching and background using the Zeiss FRAP module. Images were acquired from at least two separate experiments. Graphing analysis and curve fitting was performed using Graphpad Prism and FRAPAnalyser (Halavatyi et al., 2009).

Immunoprecipitation assays

Cells were collected in PBS and lysed in 10 volumes of 50 mM Tris-HCl at pH 7.5, 2 mM EDTA, 150 mM NaCl, and 1% Triton X-100 (immunoprecipitation buffer) followed by brief sonication. Where indicated, cells were first chemically crosslinked in 1 mM Dithiobis (succinimidyl propionate) before lysis. Extracts were incubated with the indicated antibodies overnight at 4°C. Protein G magnetic beads (25 µl of a 50% solution; Thermo Scientific) were added and the mixture was incubated

Journal of Cell Science

for another 2 h at 4°C. The beads were washed extensively in immunoprecipitation buffer, and eluted by boiling in SDS sample buffer. Immunoprecipitation assays with phalloidin were filtered to remove excess phalloidin before antibody was added, and beads were additionally washed with TBS to reduce non-specific binding before elution. In the GFP pulldowns, either anti-GFP antibody or GFP-Trap magnetic beads were used. GFP-Trap beads (20 µl of a 50% solution; Chromotek) were incubated in cell lysate for 4 h at 4°C instead of antibody or protein G.

Sedimentation assays

Nuclei were purified by incubating cells in hypotonic buffer (10 mM HEPES pH 7.9, 1.5 mM $MgCl_2$, 10 mM KCl, 0.5 mM DTT) followed by mechanical perturbation through a 25 g needle. Isolated nuclei were then lysed in transcription buffer (20 mM HEPES pH 7.9, 20% glycerol, 100 mM KCl, 0.2 mM EDTA, 0.5 mM PMSF and 0.5 mM DTT) with a 30 g needle and cleared by centrifugation (10 min at 10,000 ***g***). To perform sedimentation assays, extracts were spun at 100,000 ***g*** for 1 h at 10°C. Soluble fractions were directly boiled in hot SDS. Pellets were sonicated in hot SDS to ensure complete suspension.

Molecular brightness analyses

Brightness of the expressed constructs was extracted from a number and brightness analysis performed as previously described (Digman et al., 2008). Time-sequences (100 frames) of raster scan images were collected using an Olympus FV1000 Confocal Microscope, using the following parameters: pixel dwell time, 8 µs; frame size, 256×256 pixels; photon counting detection; excitation wavelength 488 nm (1 and 2) and/or 515 nm (2 and 3). Power level at the sample were: 1.2 µW at 488 nm and 3.3 µW at 515 nm. Emission filters were: DM 488/453/633, BA 505–605 bp (at 488 nm excitation) and DM 405-400/515, BA 535–565 bp (at 515 nm excitation).

The molecular brightness for each pixel of the image was calculated according to published protocols and software (Globals for Images). Briefly, molecular brightness is defined as $B=\sigma^2/(S^*)$, where σ^2 is the variance of the fluorescence signal measured in a pixel over time, is the average intensity and S (S=5) is a correction factor to account for the fact that the detector is not an ideal photon-counting module. The average brightness from all the pixels of the image of the nucleus that do not contain any filament or bright structure is used to provide the B-value of a given cell. Under the experimental conditions employed, the brightness of monomeric EGFP and EYFP appeared to be comparable (Storti et al., 2012).

RNAPII foci size analyses

Transfected cells were stained with anti-RNAPII antibody. Individual nuclei images were thresholded to identify single fluorescence foci using the find maximum function, and the relative area of these foci (as a measure of number of pixels) was obtained using ImageJ.

ChIP-qPCR

HeLa cells transfected with EGFP or actin constructs were treated with 100 ng/ml recombinant Interferon-γ (Invitrogen) 16 h before harvesting. Cells were then collected in cold PBS and lysed in 5 mM PIPES pH 8.0, 85 mM KCL, 0.5% NP-40, 0.5 mM PMSF plus protease inhibitor cocktail and phosphatase inhibitor cocktail (Sigma-Aldrich). Nuclei were pelleted and re-suspended in formaldehyde buffer [5 mM PIPES pH 8.0, 85 mM KCL, 1% formaldehyde (Sigma-Aldrich)], 0.5 mM PMSF plus protease inhibitor cocktail and phosphatase inhibitor cocktail for 13 min at room temperature. The reaction was quenched with 67 mM glycine for 5 m. Fixed nuclei were pelleted and washed in 5 mM PIPES pH 8.0, 85 mM KCl, 0.5 mM PMSF plus protease and phosphatase inhibitor cocktails. Nuclei were pelleted by centrifugation and resuspended in 0.5% SDS, 10 mM EDTA, 50 mM Tris-HCl pH 7.5, 0.5 mM PMSF plus protease and phosphatase inhibitor cocktails. Following sonication to generate 200–600-bp DNA fragments, nuclear extracts were diluted 10× with antibody binding buffer (0.01% SDS, 1.1% Triton X-100, 1.2 mM EDTA, 16.7 mM Tris-HCl pH 8.1, 167 mM NaCl, 0.5 mM PMSF plus protease and phosphatase inhibitor cocktails). 5 µg anti-RNAPII (4H8) antibody was added to each sample and incubated overnight at 4°C. Antibody-bound protein–DNA complexes were captured by adding 25 µl of Dynabeads Protein G (Thermo Scientific) for 2 h at 4°C. The complexes were washed (1 ml) once with low-salt buffer (0.1% SDS, 1% Triton X-100, 2 mM EDTA, 20 mM Tris pH 8.1, 150 mM NaCl), once with high-salt buffer (same buffer made 500 mM NaCl), once with LiCl wash buffer (0.25 M LiCl, 1% NP-40, 1 mM EDTA, 10 mM Tris pH 8.0), and twice with TE buffer. 10% Chelex-100 (Biorad) was added to input samples and washed beads to recover DNA and boiled for 15 min at 100°C. 20 µg/ml Proteinase K (Thermo Scientific) was added for 30 min at 55°C with shaking. Proteinase K was inactivated by boiling for 10 min. Quantitative PCR (qPCR) analysis was conducted using iQ Sybr Green reagent (Biorad). Primers for the MHCIITA promoter (5′-GCCTCCAGTCGGTTCCTCAC-AG and 5′-CACGGTTGGACTGAGTTGGAGAGA) were used. qPCR was run at 95°C for 3 min then 40 cycles of 95°C for 20 s and 63°C for 40 s. Ct values were normalized to total input.

Luciferase assay

The MAL/SRF luciferase reporter (Baarlink et al., 2013) and the MHCIITA promoter luciferase construct (Hofmann et al., 2004) were used as described previously. Luciferase activity (RLU) was normalized to luciferase activity in EGFP co-transfected cells. For MHCIITA promoter induction, COS7 cells were treated with 500 U Interferon-γ (Sigma-Aldrich) overnight. RLU was normalized to protein concentration and cell transfected with MHCIITA-driven luciferase alone.

BrU and BrDU incorporation assay

COS7 cells were grown on glass coverslips and transiently transfected for 48 h then incubated with 10 µM BrdU for 5 h or 2 mM BrU for 2 h. Cells were fixed in 4% PFA and permeabilized in 0.3% Triton X-100. In the case of BrdU incorporation, cells were then incubated in 2 M HCl for 30 m and neutralized in phosphate buffer. Cells were subsequently stained with anti-BrdU antibody and imaged with an epifluorescent microscope. Fluorescence intensity was quantified using Image J. Fluorescence was normalized to non-transfected cells in each frame.

In vitro transcription assay

In vitro transcription assays were performed as previously described (Hofmann et al., 2004). Briefly, purified HeLa nuclear extract (30 µg, Promega) in transcription buffer (20 mM HEPES pH 7.9, 20% glycerol, 100 mM KCl, 0.2 mM EDTA, 0.5 mM PMSF, and 0.5 mM DTT) with 1 mM ATP and 4 mM $MgCl_2$ was pre-incubated with 0.5 µM purified ACD (Kudryashov et al., 2008) or buffer alone for 1 h at room temperature or with 10 µM phalloidin for 30 min at 4°C. After pre-incubation, RNAse T1 was added, along with 200 ng P41 DNA template containing the adenoviral major late promoter and G-less transcribing region and 0.4 mM of ATP, UTP and 0.02 mM CTP. ^{32}[P]αCTP was then added to the reaction and incubated for 30 min at 30°C. mRNA transcript was purified using a Trizol–choloroform extraction and run using 6 M urea PAGE.

Acknowledgements

We thank Elizabeth Luna (University of Massachusetts Medical School) for the EGFP–supervillin constructs, Kathryn North (University of Sydney) for the α-actin–GFP constructs, Marc Vigneron (Université de Strasbourg) for the GFP–RNAPII construct, Maria Vartiainen (University of Helsinki) for the MAL/SRF construct, Teng-Leong Chew (Janelia Farm) for help with SIM microscopy, and the UIC Research Resource Center for help in imaging and DNA sequencing.

Competing interests

The authors declare no competing or financial interests.

Author contributions

L.A.S. and P.deL. conceived of experiments; L.A.S., M.P., P.A., C.M.C. and K.L. conducted experiments. E.G., D.S.K., S.T.K., C.J.G. and P.deL. supervised and/or contributed to the design of experiments; L.A.S., G.J.G. and P.deL. analyzed the data and wrote the manuscript.

Funding

This work was supported by the National Institutes of Health (NIH) [grant numbers GM80587 to P.deL., GM076561 to C.J.G., GM114666 to D.S.K. and GM076516 and

GM103540 to E.G.]; the Chicago Biomedical Consortium with support from the Searle Funds at the Chicago Community Trust (to P.deL. and S.T.K.); the Northwestern University Physical Sciences Oncology Center associated with National Cancer Institute [grant number U54CA143869 to C.J.G., P.deL. and S.T.K.]; the American Heart Association (AHA) [grant numbers 13IRG14780028 to D.S.K. and 13PRE17050060 to L.A.S.]; a Chicago Biomedical Consortium Scholar award (to L.A.S.); a University of Illinois at Chicago (UIC) Dean's Scholar and Chancellor's graduate research fellowship (to L.A.S.); and a UIC CM Craig Fellowship (to M.P.). Deposited in PMC for release after 12 months.

Supplementary information

Supplementary information available online at
http://jcs.biologists.org/lookup/doi/10.1242/jcs.195867.supplemental

References

Baarlink, C., Wang, H. and Grosse, R. (2013). Nuclear actin network assembly by formins regulates the SRF coactivator MAL. *Science* **340**, 864-867.

Belin, B. J., Cimini, B. A., Blackburn, E. H. and Mullins, R. D. (2013). Visualization of actin filaments and monomers in somatic cell nuclei. *Mol. Biol. Cell* **24**, 982-994.

Belin, B. J., Lee, T. Mullins, R. D. (2015). DNA damage induces nuclear actin filament assembly by formin-2 and Spire-1/2 that promotes efficient DNA repair. *eLife* **4**, e07735.

Berland, K. M., So, P. T. and Gratton, E. (1995). Two-photon fluorescence correlation spectroscopy: method and application to the intracellular environment. *Biophys. J.* **68**, 694-701.

Bregman, D. B., Du, L., van der Zee, S. and Warren, S. L. (1995). Transcription-dependent redistribution of the large subunit of RNA polymerase II to discrete nuclear domains. *J. Cell Biol.* **129**, 287-298.

Brotschi, E. A., Hartwig, J. H. and Stossel, T. P. (1978). The gelation of actin by actin-binding protein. *J. Biol. Chem.* **253**, 8988-8993.

Chang, L., Godinez, W. J., Kim, I.-H., Tektonidis, M., de Lanerolle, P., Eils, R., Rohr, K. and Knipe, D. M. (2011). PNAS Plus: Herpesviral replication compartments move and coalesce at nuclear speckles to enhance export of viral late mRNA. *Proc. Natl. Acad. Sci. USA* **108**, E136-E144.

Chen, Y., Wei, L.-N. and Müller, J. D. (2003). Probing protein oligomerization in living cells with fluorescence fluctuation spectroscopy. *Proc. Natl. Acad. Sci. USA* **100**, 15492-15497.

Cisterna, B., Necchi, D., Prosperi, E. and Biggiogera, M. (2006). Small ribosomal subunits associate with nuclear myosin and actin in transit to the nuclear pores. *FASEB J.* **20**, 1901-1903.

Courtemanche, N., Pollard, T. D. and Chen, Q. (2016). Avoiding artefacts when counting polymerized actin in live cells with LifeAct fused to fluorescent proteins. *Nat. Cell Biol.* **18**, 676-683.

Darzacq, X., Shav-Tal, Y., de Turris, V., Brody, Y., Shenoy, S. M., Phair, R. D. and Singer, R. H. (2007). In vivo dynamics of RNA polymerase II transcription. *Nat. Struct. Mol. Biol.* **14**, 796-806.

Daugherty, R. L., Serebryannyy, L., Yemelyanov, A., Flozak, A. S., Yu, H.-J., Kosak, S. T., deLanerolle, P. and Gottardi, C. J. (2014). alpha-Catenin is an inhibitor of transcription. *Proc. Natl. Acad. Sci. USA* **111**, 5260-5265.

de Lanerolle, P. (2012). Nuclear actin and myosins at a glance. *J. Cell Sci.* **125**, 4945-4949.

de Lanerolle, P. and Serebryannyy, L. (2011). Nuclear actin and myosins: life without filaments. *Nat. Cell Biol.* **13**, 1282-1288.

Digman, M. A., Dalal, R., Horwitz, A. F. and Gratton, E. (2008). Mapping the number of molecules and brightness in the laser scanning microscope. *Biophys. J.* **94**, 2320-2332.

Domazetovska, A., Ilkovski, B., Cooper, S. T., Ghoddusi, M., Hardeman, E. C., Minamide, L. S., Gunning, P. W., Bamburg, J. R. and North, K. N. (2007a). Mechanisms underlying intranuclear rod formation. *Brain* **130**, 3275-3284.

Domazetovska, A., Ilkovski, B., Kumar, V., Valova, V. A., Vandebrouck, A., Hutchinson, D. O., Robinson, P. J., Cooper, S. T., Sparrow, J. C., Peckham, M. et al. (2007b). Intranuclear rod myopathy: molecular pathogenesis and mechanisms of weakness. *Ann. Neurol.* **62**, 597-608.

Dopie, J., Skarp, K.-P., Rajakyla, E. K., Tanhuanpaa, K. and Vartiainen, M. K. (2012). Active maintenance of nuclear actin by importin 9 supports transcription. *Proc. Natl. Acad. Sci. USA* **109**, E544-E552.

Dopie, J., Rajakyla, E. K., Joensuu, M. S., Huet, G., Ferrantelli, E., Xie, T., Jaalinoja, H., Jokitalo, E. and Vartiainen, M. K. (2015). Genome-wide RNAi screen for nuclear actin reveals a network of cofilin regulators. *J. Cell Sci.* **128**, 2388-2400.

Du, J., Fan, Y. L., Chen, T. L. and Feng, X. Q. (2015). Lifeact and Utr230 induce distinct actin assemblies in cell nuclei. *Cytoskeleton (Hoboken)* **72**, 570-575.

Egly, J. M., Miyamoto, N. G., Moncollin, V. and Chambon, P. (1984). Is actin a transcription initiation factor for RNA polymerase B? *EMBO J.* **3**, 2363-2371.

Fang, Z. and Luna, E. J. (2013). Supervillin-mediated suppression of p53 protein enhances cell survival. *J. Biol. Chem.* **288**, 7918-7929.

Feric, M. and Brangwynne, C. P. (2013). A nuclear F-actin scaffold stabilizes ribonucleoprotein droplets against gravity in large cells. *Nat. Cell Biol.* **15**, 1253-1259.

Fuchsova, B., Serebryannyy, L. A. and de Lanerolle, P. (2015). Nuclear actin and myosins in adenovirus infection. *Exp. Cell Res.* **338**, 170-182.

Gettemans, J., Van Impe, K., Delanote, V., Hubert, T., Vandekerckhove, J. and De Corte, V. (2005). Nuclear actin-binding proteins as modulators of gene transcription. *Traffic* **6**, 847-857.

Goley, E. D., Ohkawa, T., Mancuso, J., Woodruff, J. B., D'Alessio, J. A., Cande, W. Z., Volkman, L. E. and Welch, M. D. (2006). Dynamic nuclear actin assembly by Arp2/3 complex and a baculovirus WASP-like protein. *Science* **314**, 464-467.

Gonsior, S. M., Platz, S., Buchmeier, S., Scheer, U., Jockusch, B. M. and Hinssen, H. (1999). Conformational difference between nuclear and cytoplasmic actin as detected by a monoclonal antibody. *J. Cell Sci.* **112**, 797-809.

Goodson, H. V. and Hawse, W. F. (2002). Molecular evolution of the actin family. *J. Cell Sci.* **115**, 2619-2622.

Grosse, R. and Vartiainen, M. K. (2013). To be or not to be assembled: progressing into nuclear actin filaments. *Nat. Rev. Mol. Cell Biol.* **14**, 693-697.

Halavatyi, A. A., Nazarov, P. V., Medves, S., van Troys, M., Ampe, C., Yatskou, M. and Friederich, E. (2009). An integrative simulation model linking major biochemical reactions of actin-polymerization to structural properties of actin filaments. *Biophys. Chem.* **140**, 24-34.

Ho, C. Y., Jaalouk, D. E., Vartiainen, M. K. and Lammerding, J. (2013). Lamin A/C and emerin regulate MKL1–SRF activity by modulating actin dynamics. *Nature* **497**, 507-511.

Hofmann, W. A., Stojiljkovic, L., Fuchsova, B., Vargas, G. M., Mavrommatis, E., Philimonenko, V., Kysela, K., Goodrich, J. A., Lessard, J. L., Hope, T. J. et al. (2004). Actin is part of pre-initiation complexes and is necessary for transcription by RNA polymerase II. *Nat. Cell Biol.* **6**, 1094-1101.

Hofmann, W. A., Vargas, G. M., Ramchandran, R., Stojiljkovic, L., Goodrich, J. A. and de Lanerolle, P. (2006). Nuclear myosin I is necessary for the formation of the first phosphodiester bond during transcription initiation by RNA polymerase II. *J. Cell Biochem.* **99**, 1001-1009.

Hofmann, W. A., Richards, T. A. and de Lanerolle, P. (2009). Ancient animal ancestry for nuclear myosin. *J. Cell Sci.* **122**, 636-643.

Hu, P., Wu, S. and Hernandez, N. (2004). A role for beta-actin in RNA polymerase III transcription. *Genes Dev.* **18**, 3010-3015.

Johnson, M. A., Sharma, M., Mok, M. T. S. and Henderson, B. R. (2013). Stimulation of in vivo nuclear transport dynamics of actin and its co-factors IQGAP1 and Rac1 in response to DNA replication stress. *Biochim. Biophys. Acta* **1833**, 2334-2347.

Kapoor, P. and Shen, X. (2014). Mechanisms of nuclear actin in chromatin-remodeling complexes. *Trends Cell Biol.* **24**, 238-246.

Kokai, E., Beck, H., Weissbach, J., Arnold, F., Sinske, D., Sebert, U., Gaiselmann, G., Schmidt, V., Walther, P., Münch, J. et al. (2014). Analysis of nuclear actin by overexpression of wild-type and actin mutant proteins. *Histochem. Cell Biol.* **141**, 123-135.

Kudryashov, D. S., Durer, Z. A. O., Ytterberg, A. J., Sawaya, M. R., Pashkov, I., Prochazkova, K., Yeates, T. O., Loo, R. R. O., Loo, J. A., Satchell, K. J. F. et al. (2008). Connecting actin monomers by iso-peptide bond is a toxicity mechanism of the Vibrio cholerae MARTX toxin. *Proc. Natl. Acad. Sci. USA* **105**, 18537-18542.

Lin, S., Coutinho-Mansfield, G., Wang, D., Pandit, S. and Fu, X. D. (2008). The splicing factor SC35 has an active role in transcriptional elongation. *Nat. Struct. Mol. Biol.* **15**, 819-826.

Lundquist, M. R., Storaska, A. J., Liu, T.-C., Larsen, S. D., Evans, T., Neubig, R. R. and Jaffrey, S. R. (2014). Redox modification of nuclear actin by MICAL-2 regulates SRF signaling. *Cell* **156**, 563-576.

McDonald, D., Carrero, G., Andrin, C., de Vries, G. and Hendzel, M. J. (2006). Nucleoplasmic beta-actin exists in a dynamic equilibrium between low-mobility polymeric species and rapidly diffusing populations. *J. Cell Biol.* **172**, 541-552.

Miyamoto, K., Pasque, V., Jullien, J. and Gurdon, J. B. (2011). Nuclear actin polymerization is required for transcriptional reprogramming of Oct4 by oocytes. *Genes Dev.* **25**, 946-958.

Munsie, L., Caron, N., Atwal, R. S., Marsden, I., Wild, E. J., Bamburg, J. R., Tabrizi, S. J. and Truant, R. (2011). Mutant huntingtin causes defective actin remodeling during stress: defining a new role for transglutaminase 2 in neurodegenerative disease. *Hum. Mol. Genet.* **20**, 1937-1951.

Nishida, E., Iida, K., Yonezawa, N., Koyasu, S., Yahara, I. and Sakai, H. (1987). Cofilin is a component of intranuclear and cytoplasmic actin rods induced in cultured cells. *Proc. Natl. Acad. Sci. USA* **84**, 5262-5266.

Obrdlik, A. and Percipalle, P. (2011). The F-actin severing protein cofilin-1 is required for RNA polymerase II transcription elongation. *Nucleus* **2**, 72-79.

Philimonenko, V. V., Zhao, J., Iben, S., Dingová, H., Kyselá, K., Kahle, M., Zentgraf, H., Hofmann, W. A., de Lanerolle, P., Hozak, P. et al. (2004). Nuclear actin and myosin I are required for RNA polymerase I transcription. *Nat. Cell Biol.* **6**, 1165-1172.

Plessner, M. and Grosse, R. (2015). Extracellular signaling cues for nuclear actin polymerization. *Eur. J. Cell Biol.* **94**, 359-362.

Plessner, M., Melak, M., Chinchilla, P., Baarlink, C. and Grosse, R. (2015). Nuclear F-actin formation and reorganization upon cell spreading. *J. Biol. Chem.* **290**, 11209-11216.
Pollard, T. D. and Cooper, J. A. (2009). Actin, a central player in cell shape and movement. *Science* **326**, 1208-1212.
Posern, G., Sotiropoulos, A. and Treisman, R. (2002). Mutant actins demonstrate a role for unpolymerized actin in control of transcription by serum response factor. *Mol. Biol. Cell* **13**, 4167-4178.
Rungger, D., Rungger-Brändle, E., Chaponnier, C. and Gabbiani, G. (1979). Intranuclear injection of anti-actin antibodies into Xenopus oocytes blocks chromosome condensation. *Nature* **282**, 320-321.
Sacco-Bubulya, P. and Spector, D. L. (2002). Disassembly of interchromatin granule clusters alters the coordination of transcription and pre-mRNA splicing. *J. Cell Biol.* **156**, 425-436.
Scheer, U., Hinssen, H., Franke, W. W. and Jockusch, B. M. (1984). Microinjection of actin-binding proteins and actin antibodies demonstrates involvement of nuclear actin in transcription of lampbrush chromosomes. *Cell* **39**, 111-122.
Sen, B., Xie, Z., Uzer, G., Thompson, W. R., Styner, M., Wu, X. and Rubin, J. (2015). Intranuclear actin regulates osteogenesis. *Stem Cells* **33**, 3065-3076.
Serebryannyy, L. A., Cruz, C. M. and de Lanerolle, P. (2016). A role for nuclear actin in HDAC 1 and 2 regulation. *Sci. Rep.* **6**, 28460.
Spencer, V. A., Costes, S., Inman, J. L., Xu, R., Chen, J., Hendzel, M. J. and Bissell, M. J. (2011). Depletion of nuclear actin is a key mediator of quiescence in epithelial cells. *J. Cell Sci.* **124**, 123-132.
Spracklen, A. J., Fagan, T. N., Lovander, K. E. and Tootle, T. L. (2014). The pros and cons of common actin labeling tools for visualizing actin dynamics during Drosophila oogenesis. *Dev. Biol.* **393**, 209-226.
Stenzel, W., Preusse, C., Allenbach, Y., Pehl, D., Junckerstorff, R., Heppner, F. L., Nolte, K., Aronica, E., Kana, V., Rushing, E. et al. (2015). Nuclear actin aggregation is a hallmark of anti-synthetase syndrome-induced dysimmune myopathy. *Neurology* **84**, 1346-1354.
Storti, B., Bizzarri, R., Cardarelli, F. and Beltram, F. (2012). Intact microtubules preserve transient receptor potential vanilloid 1 (TRPV1) functionality through receptor binding. *J. Biol. Chem.* **287**, 7803-7811.
Sugaya, K., Vigneron, M. and Cook, P. R. (2000). Mammalian cell lines expressing functional RNA polymerase II tagged with the green fluorescent protein. *J. Cell Sci.* **113**, 2679-2683.
Ting, H.-J., Yeh, S., Nishimura, K. and Chang, C. (2002). Supervillin associates with androgen receptor and modulates its transcriptional activity. *Proc. Natl. Acad. Sci. USA* **99**, 661-666.
Vartiainen, M. K., Guettler, S., Larijani, B. and Treisman, R. (2007). Nuclear actin regulates dynamic subcellular localization and activity of the SRF cofactor MAL. *Science* **316**, 1749-1752.
Wang, I.-F., Chang, H.-Y. and James Shen, C.-K. (2006). Actin-based modeling of a transcriptionally competent nuclear substructure induced by transcription inhibition. *Exp. Cell Res.* **312**, 3796-3807.
Wulfkuhle, J. D., Donina, I. E., Stark, N. H., Pope, R. K., Pestonjamasp, K. N., Niswonger, M. L. and Luna, E. J. (1999). Domain analysis of supervillin, an F-actin bundling plasma membrane protein with functional nuclear localization signals. *J. Cell Sci.* **112**, 2125-2136.
Yahara, I., Harada, F., Sekita, S., Yoshihira, K. and Natori, S. (1982). Correlation between effects of 24 different cytochalasins on cellular structures and cellular events and those on actin in vitro. *J. Cell Biol.* **92**, 69-78.
Ye, J., Zhao, J., Hoffmann-Rohrer, U. and Grummt, I. (2008). Nuclear myosin I acts in concert with polymeric actin to drive RNA polymerase I transcription. *Genes Dev.* **22**, 322-330.

Table S1: FRAP Kinetics. (**A**) FRAP analyses of regions of diffuse EYFP-NLS-β-actin in transfected COS7 cells with (NAF Positive) or without nuclear actin filaments (NAF Negative). Data was fit to biphasic exponential recovery curves (**Fig. 1F**)**.** (**B**) FRAP analyses of GFP-RNAPII in COS7 cells stably expressing GFP-RNAPII and left non-transfected or co-transfected with mCherry-supervillin fragment (**Fig. 4F**). (**C**) FRAP analyses of MS2-GFP as a measure of the rate of transcription in U2OS-263 cells and U2OS-263 cells with nuclear actin filaments induced by mCherry-supervillin fragment (**Fig. 4G**). Means ± S.E.M. Asterisks denote statistical significance by Student's t-test.

(A) EYFP-NLS-β-Actin FRAP (Fig. 1F)	NAF Negative	NAF Positive
Mobile Fraction (%) ***	0.9192 ± 0.0065	0.7904 ± 0.0104
$T_{1/2\ fast}$	0.4971 ± 0.0771	0.5527 ± 0.0504
$T_{1/2\ slow}$ ***	17.11 ± 2.485	36.67 ± 4.305
% Fast**	74.01 ± 1.12	69.45 ± 0.63
N	17	17
R^2	0.9189	0.9718

(B) GFP-RNAPII (Fig. 4F)	Control - Small Foci	mCherry-Supervillin Frag. - Small Foci	mCherry-Supervillin Frag. - Large Foci
Mobile Fraction (%)	0.5029 ± 0.0185	0.5341 ± 0.0314	0.5704 ± 0.0428
$T_{1/2}$	15.16 ± 5.475	25.50 ± 11.35	41.04 ± 13.64
N	22	27	41
R^2	0.7595	0.8251	0.945

(C) MS2-GFP (Fig. 4G)	Control	mCherry-Supervillin Frag.
$T_{1/2\ fast}$ *	1.996 ± 0.337	3.863 ± 0.602
$T_{1/2\ slow}$	60.41 ± 5.33	295.7 ± 199.6
% Fast	55.62 ± 2.45	44.50 ± 8.20
N	14	14
R^2	0.9443	0.9096

Journal of Cell Science • Supplementary information

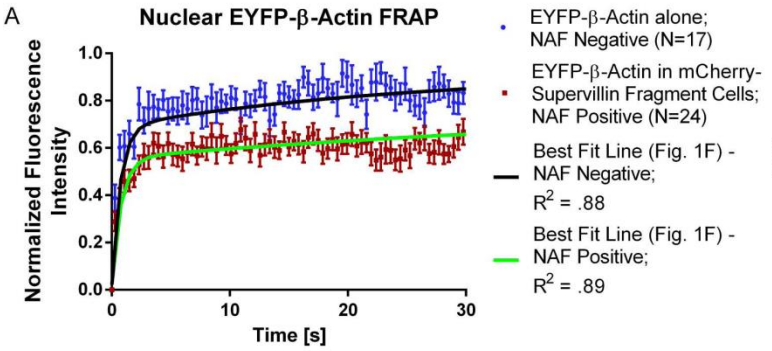
A
Nuclear EYFP-β-Actin FRAP
Normalized Fluorescence Intensity
Time [s]
EYFP-β-Actin alone; NAF Negative (N=17)
EYFP-β-Actin in mCherry-Supervillin Fragment Cells; NAF Positive (N=24)
Best Fit Line (Fig. 1F) - NAF Negative; R2 = .88
Best Fit Line (Fig. 1F) - NAF Positive; R2 = .89

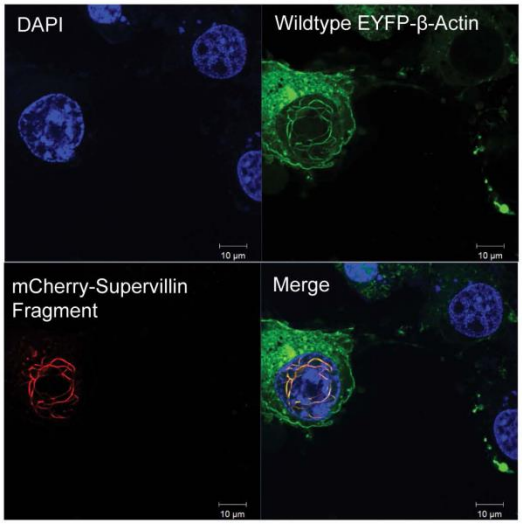
B
DAPI
Wildtype EYFP-β-Actin
mCherry-Supervillin Fragment
Merge

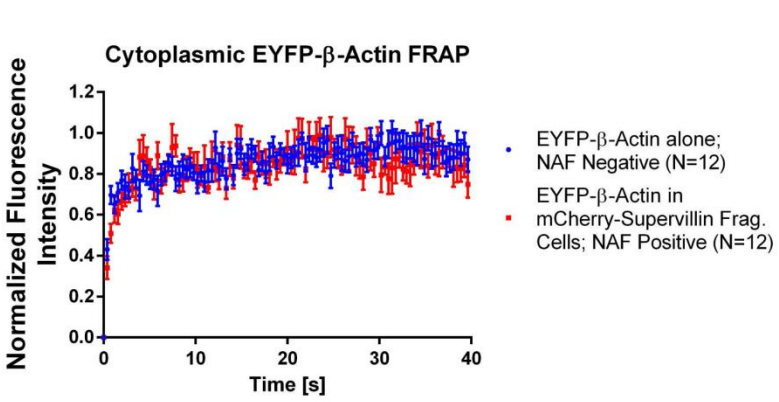
C
Cytoplasmic EYFP-β-Actin FRAP
Normalized Fluorescence Intensity
Time [s]
EYFP-β-Actin alone; NAF Negative (N=12)
EYFP-β-Actin in mCherry-Supervillin Frag. Cells; NAF Positive (N=12)

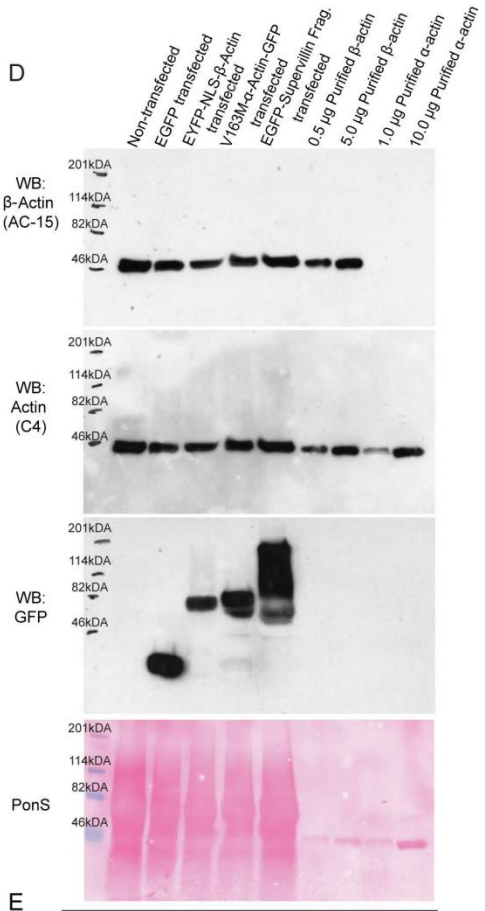
D
Non-transfected
EGFP transfected
EYFP-NLS-β-Actin transfected
V163M-α-Actin-GFP transfected
EGFP-Supervillin Frag. transfected
0.5 µg Purified β-actin
5.0 µg Purified β-actin
1.0 µg Purified α-actin
10.0 µg Purified α-actin
WB: β-Actin (AC-15)
WB: Actin (C4)
WB: GFP
PonS
201kDA
114kDA
82kDA
46kDA

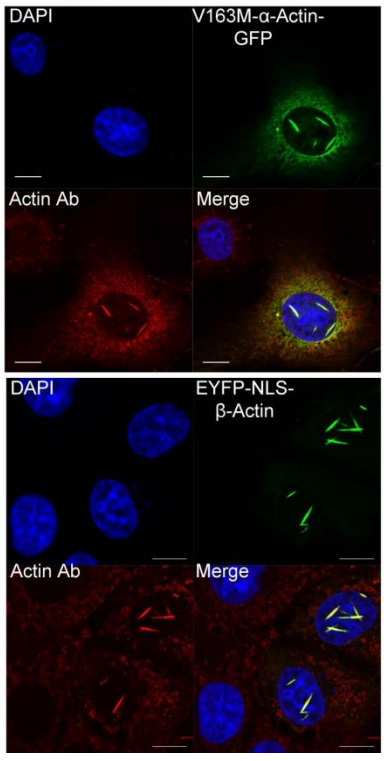
E
DAPI
V163M-α-Actin-GFP
Actin Ab
Merge
DAPI
EYFP-NLS-β-Actin
Actin Ab
Merge

Figure S1: Effects of nuclear actin filaments on cytoplasmic and nucleoplasmic actin. (**A**) FRAP experiment performed on COS7 cells transfected with wildtype EYFP-β-actin or co-transfected with wildtype β-actin EYFP and mCherry-supervillin fragment for 48 h. Areas of diffuse EYFP-β-actin were bleached in cells only expressing EYFP-β-actin (nuclear actin filament negative) and those that were also expressing mCherry-supervillin fragment and had nuclear actin filaments (nuclear actin filament positive). FRAP analysis of nuclear pools of EYFP-β-actin were fit to the biphasic exponential recovery curves calculated for EYFP-NLS-β-actin transfected cells (**Fig. 1F**). Shown are data means ± S.E.M. Nuclear actin filament negative conditions fit with a R^2 = .88, and nuclear actin filament positive fit with a R^2 = .89 (mCherry-supervillin fragment co-transfected). (**B**) COS7 cell co-transfected with wildtype EYFP-β-actin and mCherry-supervillin fragment and stained with DAPI. Note the co-localization of EYFP-β-actin and mCherry-supervillin fragment (yellow). (**C**) FRAP analysis performed as in (A) in diffuse regions of the cytoplasm in cells transfected with wildtype EYFP-β-actin or co-transfected with wildtype EYFP-β-actin and mCherry-supervillin fragment for 48 h. (**D**) Representative western blots of COS7 cells both non-transfected and transfected with nuclear actin filament forming constructs as well as purified non-muscle β-actin and skeletal α-actin. Note the poor recognition of the tested antibodies to exogenously expressed actin. (**E**) COS7 cells co-transfected with V163M-α-actin-GFP or EYFP-NLS-β-actin, fixed with ethanol to expose actin epitopes within filaments, and stained with anti-actin (C4) to mark endogenous actin. Note the presence of endogenous actin within the filaments.

Journal of Cell Science • Supplementary information

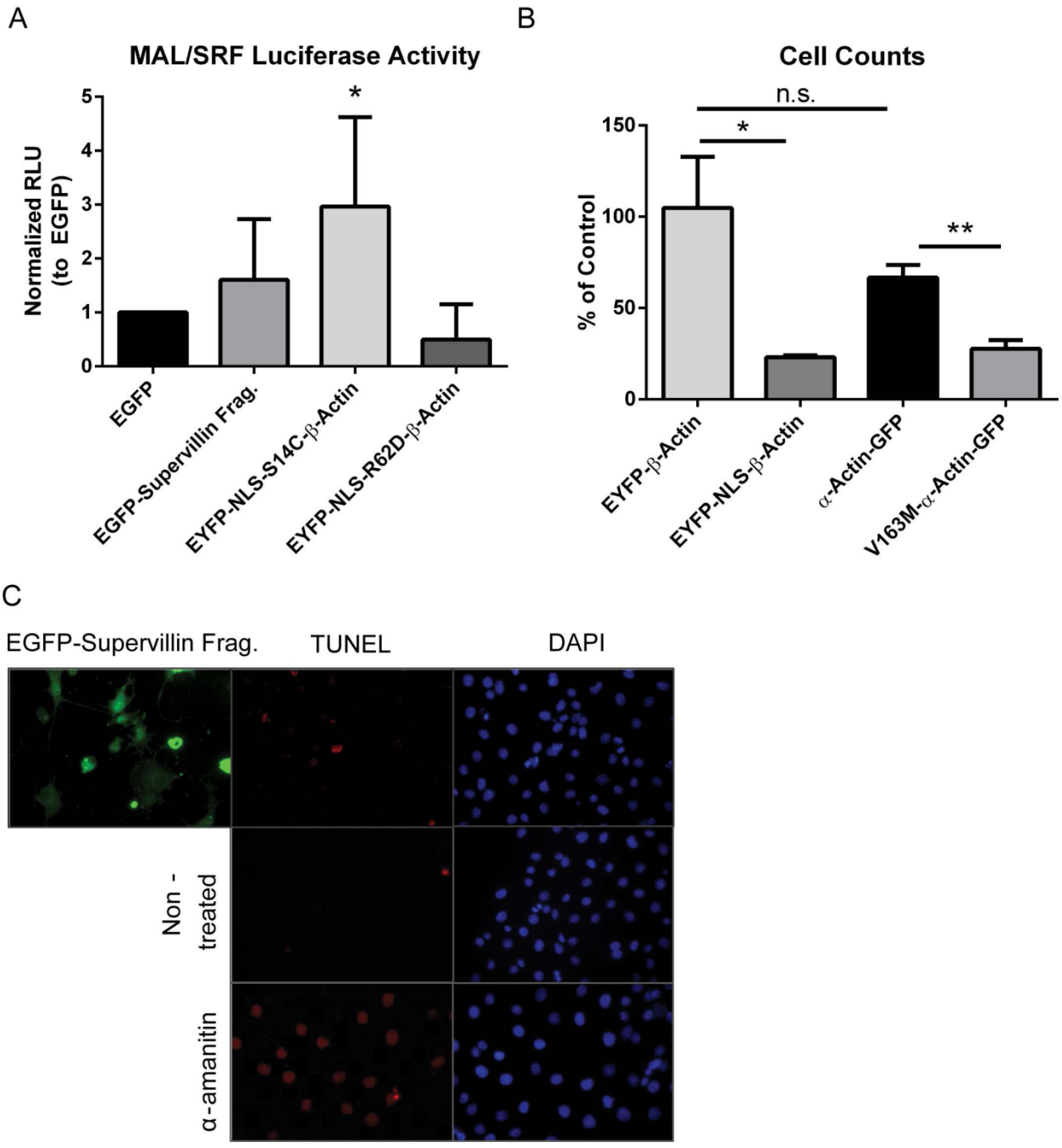

Figure S2: Effects of nuclear actin filaments on SRF/MAL activity, cell proliferation and apoptosis. (**A**) Luciferase assay of a MAL/SRF dependent promoter in cells expressing NLS-S14C/R62D-β-actin mutants, EGFP-supervillin fragment, or EGFP as a control. Relative luciferase units (RLU) were calculated after serum starvation for 24 h and stimulation for 7 h. RLU

Journal of Cell Science • Supplementary information

was normalized to cells transfected with only the luciferase construct and EGFP. N=6. Mean + S.E.M. *p<0.05, by 1-way ANOVA. (**B**) Counts of cell numbers transfected for 48 h and normalized to non-transfected cells confirm decreased proliferation in cells expressing nuclear actin filaments. N=3. Mean + S.E.M. **p<0.01,*p<0.05, n.s. - not significant by t-test. (**C**) TUNEL assay (red) of control cells, transcriptionally inhibited cells (α-amanitin), and EGFP-supervillin fragment transfected cells.

Journal of Cell Science • Supplementary information

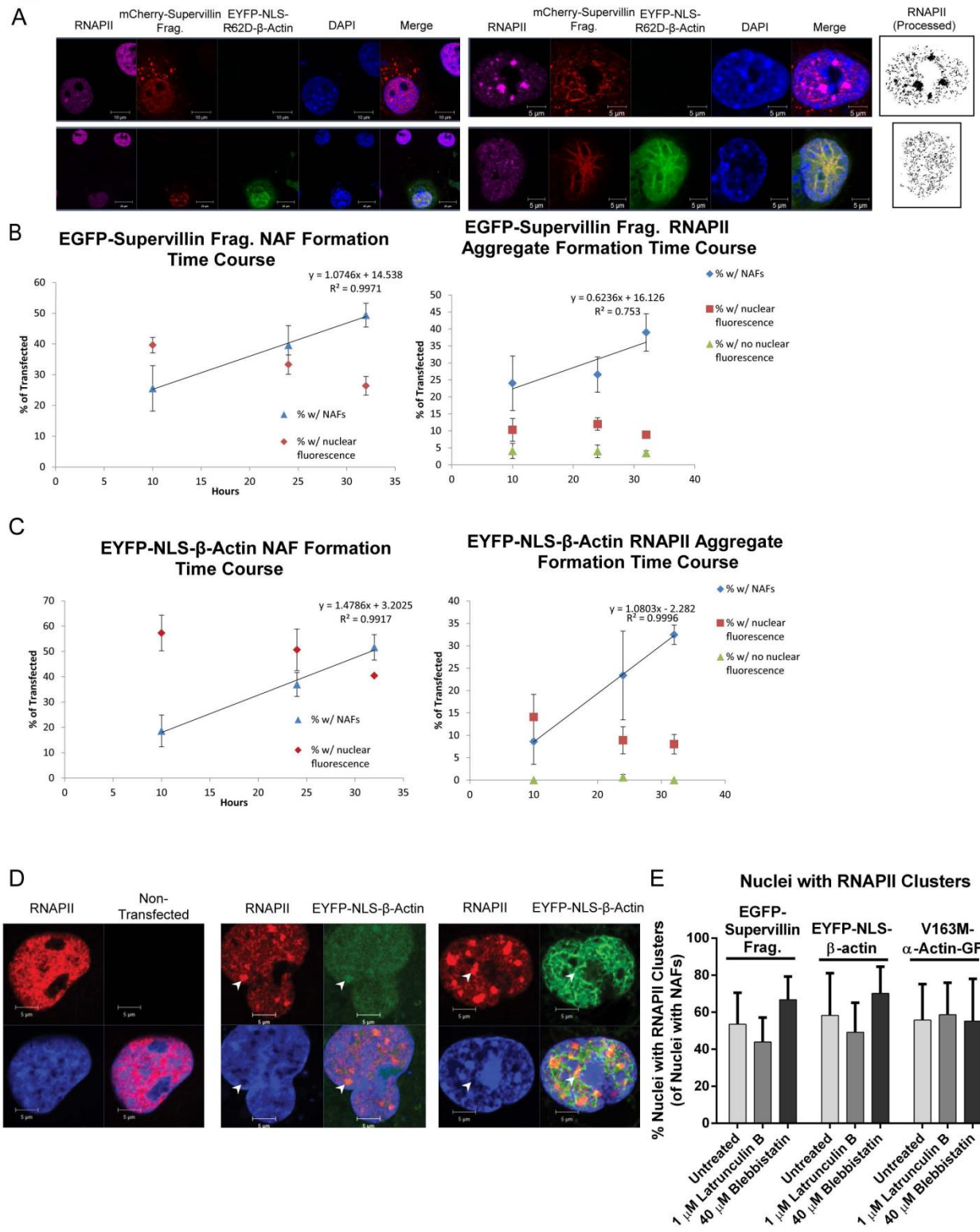
A
RNAPII
mCherry-Supervillin Frag.
EYFP-NLS-R62D-β-Actin
DAPI
Merge
RNAPII
mCherry-Supervillin Frag.
EYFP-NLS-R62D-β-Actin
DAPI
Merge
RNAPII (Processed)
B
EGFP-Supervillin Frag. NAF Formation Time Course
y = 1.0746x + 14.538
R² = 0.9971
% of Transfected
Hours
% w/ NAFs
% w/ nuclear fluorescence
EGFP-Supervillin Frag. RNAPII Aggregate Formation Time Course
y = 0.6236x + 16.126
R² = 0.753
% of Transfected
% w/ NAFs
% w/ nuclear fluorescence
% w/ no nuclear fluorescence
C
EYFP-NLS-β-Actin NAF Formation Time Course
y = 1.4786x + 3.2025
R² = 0.9917
% of Transfected
Hours
% w/ NAFs
% w/ nuclear fluorescence
EYFP-NLS-β-Actin RNAPII Aggregate Formation Time Course
y = 1.0803x - 2.282
R² = 0.9996
% of Transfected
% w/ NAFs
% w/ nuclear fluorescence
% w/ no nuclear fluorescence
D
RNAPII
Non-Transfected
RNAPII
EYFP-NLS-β-Actin
RNAPII
EYFP-NLS-β-Actin
E
Nuclei with RNAPII Clusters
% Nuclei with RNAPII Clusters (of Nuclei with NAFs)
EGFP-Supervillin Frag.
EYFP-NLS-β-actin
V163M-α-Actin-GFP
Untreated
1 μM Latrunculin B
40 μM Blebbistatin

Figure S3: Time course of nuclear actin filament formation and the associated changes in RNAPII. (**A**) Representative images used for analysis in **Fig. 4E** of non-transfected cells, mCherry-supervillin fragment transfected cells, and mCherry-supervillin fragment and EYFP-NLS-R62D-β-actin co-transfected cells. Large RNAPII clusters formed in mCherry-supervillin fragment transfected but not non-transfected nor EYFP-NLS-R62D-β-actin co-transfected cells. (**B**) Time course analysis of COS7 cells transfected with EGFP-supervillin fragment or (**C**) EYFP-NLS-β-actin for 10 h, 24 h, and 32 h. Formation of nuclear actin filaments (NAFs) and RNAPII clusters were scored in cells fixed at the indicated time points and expressed as a percentage of the total transfected cells counted. Cells were sorted by nuclei with nuclear actin filaments (blue; NAFs), cells with nuclear fluorescence but no visible filaments (red), or cells with only cytoplasmic fluorescence (green). N=3, >70 cells/group. Mean + S.E.M. (**D**) Representative images of the spectrum of nuclear actin filaments in a COS7 cell expressing EYFP-NLS-β-actin. Note the aggregation of RNAPII (arrowheads). (**E**) Cells transfected with the indicated constructs for 48 h were left untreated or treated with 1 μM latrunculin B or 40 μM Blebbistatin for 2 h before fixation. Cells were then stained for RNAPII (4H8 antibody) and the percentage of nuclei exhibiting RNAPII clusters in cells with nuclear actin filaments was quantified. Mean + S.D. At least 4 fields of view and 40 cells/group were counted.

Journal of Cell Science • Supplementary information

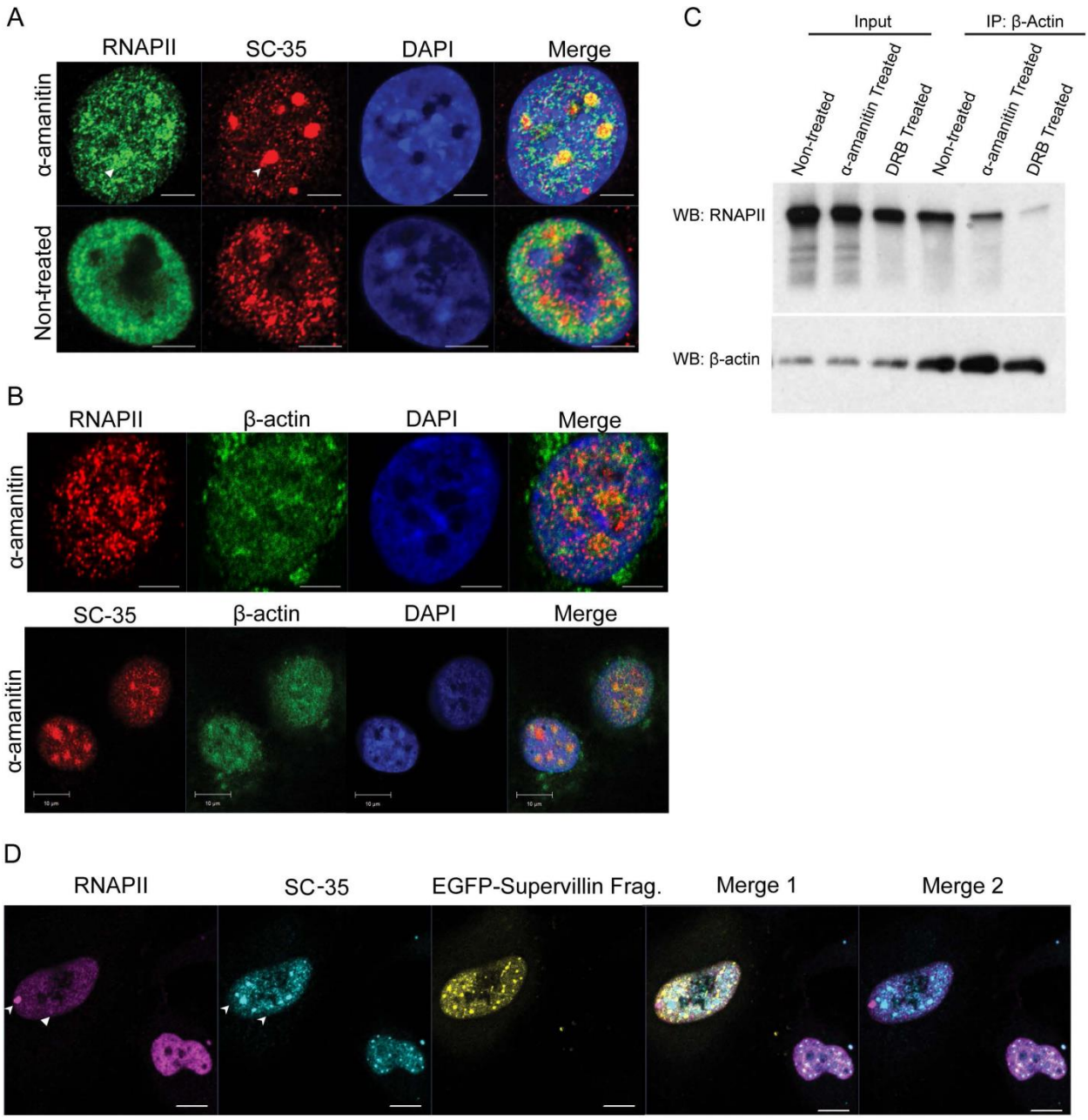

Figure S4: Direct transcription inhibition alters the RNAPII-actin interaction. (**A**) COS7 cells treated with 10 µg/ml α-amanitin overnight to inhibit transcription and stained with RNAPII (green, 4H8) and SC-35 (red) antibodies. Scale bars: 5 µm. Arrowheads indicate co-localization between RNAPII clusters and SC-35. (**B**) Confocal microscopy of COS7 cells treated with 10 µg/ml α-amanitin overnight to inhibit transcription and stained with RNAPII (red, n-20) or SC-35 (red) and β-actin (green, Ac-15) antibodies. (**C**) Co-immunoprecipitation assay of transcriptionally inhibited COS7 cells using β-actin antibody. Cells were treated with the cell-permeable crosslinker DSP before extraction. Note the decreased association of β-actin with RNAPII in transcriptionally inhibited cells. (**D**) Confocal microscopy of cells transfected with EGFP-supervillin fragment (yellow) and stained with RNAPII (magenta, 4H8) and SC-35 (cyan) antibodies. Scale bars: 10 µm. Arrowheads indicate lack of co-localization between RNAPII clusters and SC-35.